To test the effect of long-term in vitro culture, we maintained two independent GS cells for 2 years (Fig. 1A), during which the cells continued logarithmic growth. The established GS cells were weakly positive for alkaline phosphatase (Fig. 1A), and they were regularly passaged every 5 to 6 days at a dilution of 1:3 to 1:6. Every 3 months during the 24-month experimental period, representative cell samples were cryopreserved. Flow cytometric analysis after 24 months in culture showed that the GS cells expressed the spermatogonial markers β1- and α6-integrins, CD9 and EpCAM (Shinohara et al., 1999; Kanatsu-Shinohara et al., 2004a; Ryu et al., 2004); the cells weakly expressed Kit, a marker of differentiated spermatogonia (Shinohara et al., 2000), and did not express SSEA-1, an ES cell marker (Solter and Knowles, 1978) (Fig. 1B). Similarly, RT-PCR analysis after 24 months of culture showed that, although the GS cells expressed the ES cell markers Oct4, Rex1 and ERas, they did not express other ES-specific markers, such as Nanog (Pesce and Schöler, 2001; Mitsui et al., 2003; Takahashi et al., 2003; Chambers et al., 2003). By contrast, many spermatogonia or germ cell markers, including neurogenin 3, Ret, Stra8 (spermatogonia markers) (Meng et al., 2000; Giuili et al., 2002; Yoshida et al., 2004), Mvh and Stella (germ cell markers) (Fujiwara et al., 1994; Saitou et al., 2002), were expressed in the GS cells. Both PLZF and TAF4b, transcription factors involved in spermatogonial stem cell renewal (Buaas et al., 2004, Costoya et al., 2004; Falender et al., 2005), were also expressed in the GS cells (Fig. 1C). Thus, the overall morphology and marker expression profiles of the GS cells, as examined by flow cytometry and RT-PCR, did not change after an approximately 10^{85}-fold expansion by 139 passages over a 24-month period (Fig. 1E).

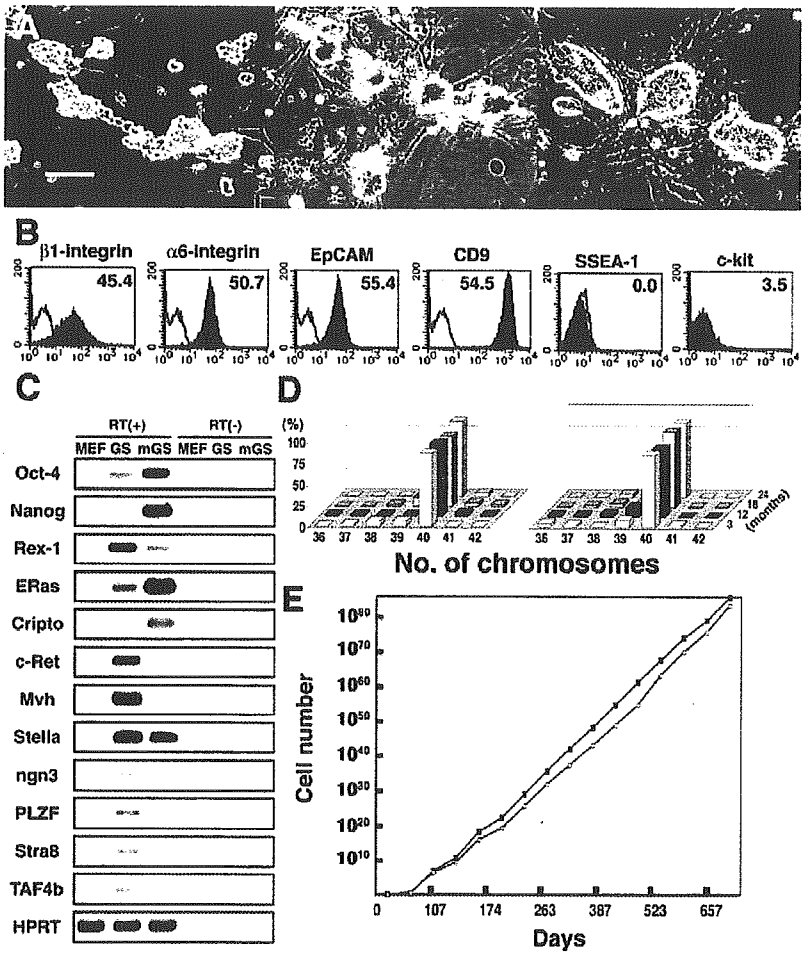

Fig. 1. Phenotypic analysis of GS cells. (A) Left, appearance of GS cells, 24 months after initiation of the cultures; middle, alkaline phosphatase activity in the GS cells; right, appearance of mGS cells that closely resemble ES cells. (B) Flow cytometric characterization of GS cells after 24 months in culture. Black line, control immunoglobulin; red line, specific antibody. (C) RT-PCR analysis. Specific primers were used to amplify cDNA from GS and mGS cells. (D) Karyotype analysis of two separate cultures of GS cells. At least 50 cells were counted. (E) Cumulative growth curves for two separate cultures of GS cells. Cells were maintained for 2 years in which the total number of cells at each passage has been calculated. There is steady and consistent exponential increase in total cell number over time. Scale bar: 100 μm in A.

Although the GS cells continued to proliferate without noticeable changes in either of the two independent cultures over the 24-month experimental period, ES-like cells (mGS cells) developed in one case after freeze-thaw treatment (Kanatsu-Shinohara et al., 2004b) (Fig. 1A). In this case, the cultured cells were divided into two fractions at 51 days after the initiation of the culture. Some of the cells were maintained for the 2-year period without cryopreservation, whereas the remaining cells were cryopreserved. In one of the cultures derived from the frozen cell stocks, mGS cells appeared 46 days after thawing, a total of 91 days from the initiation of culture. However, we did not find ES-like cells in any other of the more than 30 freeze-thaw-treated GS cell cultures, suggesting that the freeze-thaw procedure per se does not always induce the production of mGS cells. Consistent with our previous study (Kanatsu-Shinohara et al., 2004b), the mGS cells exhibited ES cell markers (Fig. 1C) and produced teratomas by subcutaneous injection into nude mice (data not shown).

Genetic and epigenetic stability of GS cells

We next examined the stability of the karyotype and imprinting patterns of the GS cells. Hoechst 33258-stained GS cells from the two independent cultures were cytogenetically analyzed at 3, 12, 18 and 24 months after the initiation of cultures. More than 80% of the cells were euploid (38 paired autosomes and two sex chromosomes) after 24 months, and the proportion of euploid metaphase cells did not change significantly during long-term culture (Fig. 1D). We also examined whether the GS cells maintained normal telomere length, as continuous cell

division generally induces shortening of the telomeres of cultured cells, eventually leading to cell cycle arrest or apoptosis (Rubin, 2002). To monitor telomere shortening, we performed Southern blot analysis to examine the TRFs that contain the telomeric repeat sequences. The telomere length in the GS cells decreased progressively at a constant rate (~0.7 kb per month) during the experimental period and was reduced to ~40% of the original length after 24 months of continuous culture (Fig. 2A,B). This occurred despite evidence of telomerase activity in GS cells (Fig. 2C).

We also determined the genomic imprinting pattern in the GS cells, because the methylation patterns of germline cells tend to change during culture. The methylation patterns of the DMRs of three paternally methylated regions [*H19*, *Meg3 IG* (Gtl2 – Mouse Genome Informatics) and *Rasgrf1*] and two maternally methylated regions (*Igf2r* and *Peg10*) were examined in GS cells harvested after 3, 12, 18 and 24 months of continuous culture (Fig. 3). Consistent with the findings of our previous study (Kanatsu-Shinohara et al., 2004b), COBRA analysis of the GS cells demonstrated androgenetic imprinting: methylation of the paternal DMRs and demethylation of the maternal DMRs. This androgenetic pattern was not altered in the two cultures at 24 months, indicating that GS cells are epigenetically stable. By contrast, the mGS cells that developed in a 3-month-old culture after freeze-thaw treatment had a different methylation pattern. Although paternally methylated regions in *H19* and *Rasgrf1* were highly methylated, DMRs in the *Meg3 IG* region were slightly undermethylated compared with those in the GS cells. Furthermore, while DMRs in *Igf2r* are unmethylated in the GS cells, they are hypermethylated in the mGS cells. These results support our previous observation that genomic imprinting is variable in mGS cells (Kanatsu-Shinohara et al., 2004).

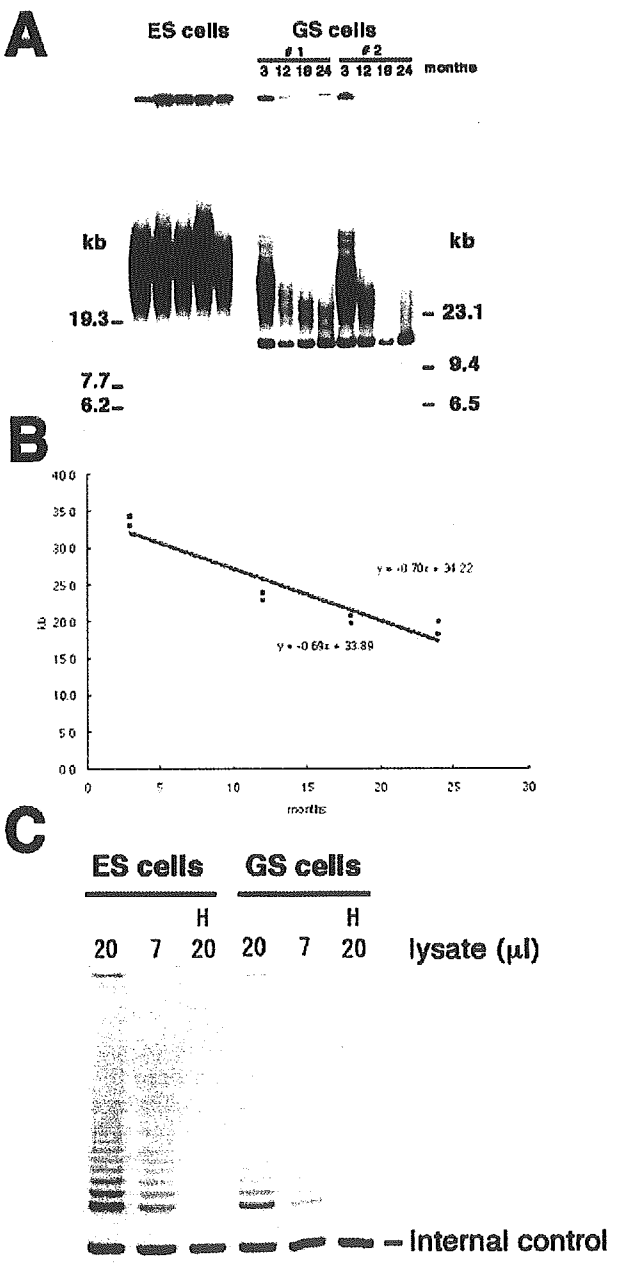

Spermatogenesis and generation of offspring from GS cells after long-term culture

To examine whether the cultured cells retained spermatogonial stem cell activity, we used a spermatogonial transplantation technique that allows competent spermatogonial stem cells to colonize the empty seminiferous tubules of infertile mouse testes (Brinster and Zimmermann, 1994). GS cells were recovered from the two separate cultures at different time points during the long-term culture period, and single cell suspensions of the cells were microinjected into the seminiferous tubules of immunosuppressed infertile W mice. W mice lack endogenous spermatogenesis, owing to mutations in the Kit receptor (Ohta et al., 2003); therefore, any spermatogenesis in the recipient testes must necessarily originate from the transplanted stem cells. Two months after transplantation, the recipient mice were sacrificed, and the testes were examined for the presence of EGFP-positive colonies under UV illumination. The transplanted GS cells colonized the seminiferous tubules of W recipient testes and produced EGFP-expressing spermatogenic colonies, regardless of the amount of time the cells had been cultured (Fig. 4A). Assuming 10% colonization efficiency (Nagano et al., 1999), the concentration of functional stem cells in the cultures ranged from 0.02% to 1.6% (Table 1). Overall, the number of stem cells expanded by approximately 1.8×10^{73}-fold during 617 days in culture, during which time the total cell number increased 1.3×10^{73}-fold. Given that the neonatal testis

Fig. 2. Analysis of telomere dynamics and telomerase activity. (A) Southern blot analysis of TRFs containing telomeric DNA sequences in five different ES (E14) cells and GS cells. Genomic DNAs from ES or GS cells were digested with *Hinf*I, separated on a pulse-field gel and probed with the 5′-[^{32}P]$(T_2AG_3)_3$ telomeric DNA oligonucleotides. (B) Loss of telomeres in GS cells. Based on the median values of the TRF analysis shown in (A), shortening rates of the telomeric DNA sequences in GS cells were calculated for two separate cultures. (C) Telomerase activity in ES and GS cells. ES and GS cells were subjected to a standard telomeric repeat amplification assay. Extracts were pretreated with (H) or without heat inactivation (80°C, 10 minutes) prior to the telomerase assay. The total amount of cell lysates per assay is indicated.

normally contains approximately 34 stem cells per 10^5 cells (Shinohara et al., 2001), this result also indicates that the stem cells expanded by ~10^{86}-fold since the initiation of the cultures. Histological analysis confirmed the presence of normal-appearing spermatogenesis in the recipient testes (Fig. 4B).

Finally, to determine whether the germ cells were functionally normal, we attempted to produce offspring from long-term cultures of GS cells. We sacrificed W recipient mice that had received GS cells from 24-month-old cultures. The EGFP-expressing colonies were dissociated mechanically under UV light. Live spermatogenic cells were recovered by repeated pipetting of EGFP-positive seminiferous tubule fragments from three different recipient mice (Fig. 4C). Round spermatids were collected and microinjected into BDF1 oocytes. A total of 194 embryos were constructed, and 130 were transferred into the oviducts of pseudopregnant ICR females (Table 2). Of the 16 offspring born, 11 expressed the *Egfp* gene (Fig. 4C). The mean weight of the neonatal mice derived from GS cells was 1.7 g, and the mean placental weight was 0.15 g, both of which were within the normal ranges. COBRA analysis of tissue samples indicated that the offspring had normal imprinting patterns (Fig. 3). The offspring developed normally and became fertile as adults.

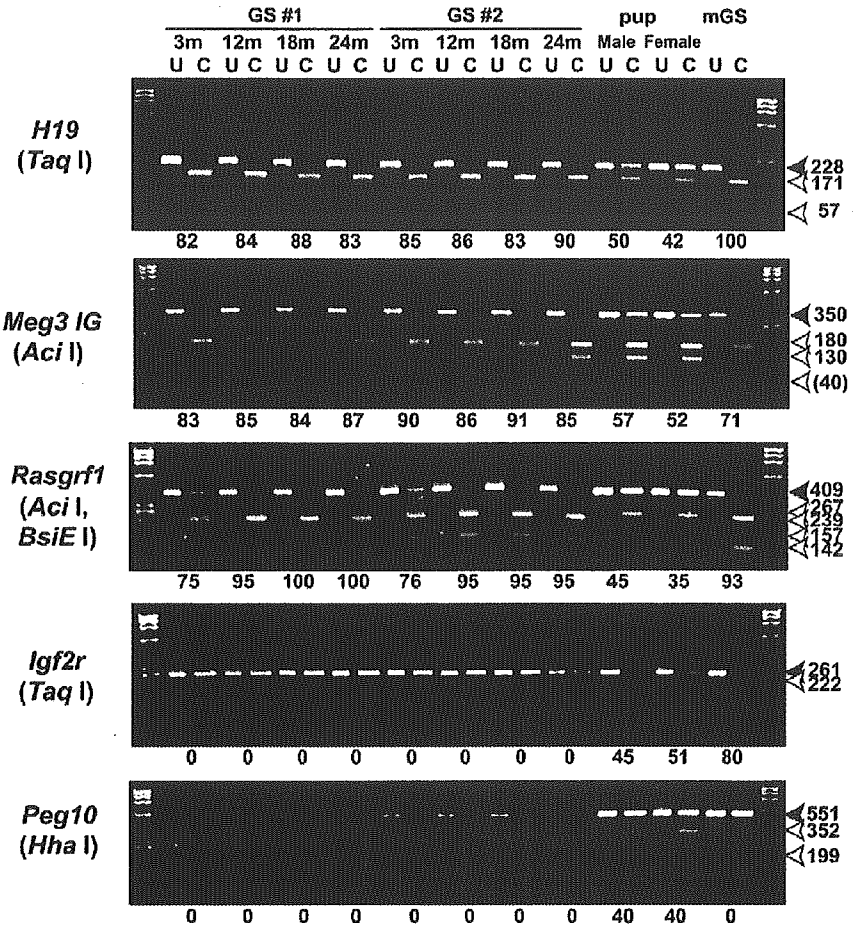

Fig. 3. COBRA of imprinted genes. PCR products of each DMR region were digested with restriction enzymes with a recognition sequence containing CpG in the original unconverted DNA. Where the enzyme sites are methylated, PCR products are fragmented; where PCR products are not fragmented, the enzyme sites are unmethylated. White arrowheads indicate the sizes of the unmethylated DNA fragments. Black arrowheads indicate the sizes of the methylated DNA fragments. The enzymes used to cleave each locus are indicated in parenthesis. *Bsi*EI was used to analyze the *Rasgrf1* DMRs in the DNA from mouse pups and from mGS cells. Levels of percentage methylation, estimated by the intensity of each band, are indicated below the gels. U, uncleaved; C, cleaved.

Discussion

Our study revealed the remarkable stability and proliferative capacity of spermatogonial stem cells during long-term culture. The genetic and epigenetic stability of spermatogonial stem cells is striking. Most mammalian somatic cells have limited proliferative potential, and eventually undergo senescence after limited number of cell divisions (Rubin, 2002). Many cells that appear after degenerative phase are aneuploid, and it is from these that the permanent cells appear to evolve (Rubin, 2002). By contrast, the growth rate of the GS cells was constant during the 2 years in culture, and the euploid karyotype was retained for at least 139 passages. Our results also showed the functional stability of cultured spermatogonial stem cells; the production of fertile offspring from cells passaged continuously for 2 years demonstrates that the functional characteristics of spermatogonial stem cells are fully retained despite long-term in vitro expansion.

Our results contrast with previous reports that demonstrated instability of germline cells in vitro. Although ES cells have a spontaneous mutation frequency that is ~100-fold below that of somatic cells (Cervantes et al., 2002), culture of germline cells, such as preimplantation embryo, ES cells and EG cells, generally induces genetic and epigenetic changes. For example, previous studies have shown that ES cells progressively lose euploidy with increasing numbers of culture passages. More than 70% of ES cells became aneuploid by passages 25 (equivalent to more than 2 months of continuous culture), and these cells could no longer contribute to the germline by blastocyst injection (Longo et al., 1997). The aneuploid abnormalities induced by long-term culture appear to occur at specific chromosome loci: whereas mouse ES cells commonly develop trisomy eight after long-term culture (Liu et al., 1997), human ES cells have trisomy 17q and 12 (Draper et al., 2004). These karyotypic changes probably confer a growth advantage in vitro and hence represent a common cause of the loss of germline potential. In addition to their chromosomal instability, in vitro culture of preimplantation

Table 1. Spermatogonial stem cell expansion during long-term culture

Culture	Days to transplant* (passage)	GS cells injected/testis ($\times 10^4$)	Colonies/testis	Colonies/ 10^5 GS cells	Stem cells/ 10^5 GS cells†	Increase in GS cell number (fold)‡	Increase in stem cell number (fold)‡,§
1	134 (24)	1.9	30.7±8.9	163.6±47.2	1635.7		
	216 (41)	7.5	1.5±0.6	2.00±0.8	20.0	1.7×10^{8}	2.1×10^{6}
	301 (58)	5.0	32.0±11.3	64.0±22.7	640.0	1.4×10^{19}	5.5×10^{18}
	366 (71)	2.7	17.7±7.5	65.4±27.9	654.4	4.7×10^{27}	1.9×10^{27}
	461 (89)	3.0	19.7±0.3	65.6±1.1	655.7	6.0×10^{39}	2.4×10^{39}
	550 (105)	1.5	9.7±1.2	64.5±8.0	644.7	5.7×10^{50}	2.3×10^{50}
	638 (121)	1.5	1.6±0.9	10.7±6.2	106.7	8.6×10^{61}	5.6×10^{60}
	730 (139)	1.5	5.5±2.3	36.7±15.0	366.7	9.1×10^{72}	2.1×10^{72}
2	113 (19)	3.0	8.7±2.1	28.9±7.1	289.0		
	216 (38)	3.75	4.7±1.0	12.5±2.6	124.5	2.1×10^{8}	9.0×10^{7}
	301 (55)	5.0	9.8±5.7	19.6±11.5	196.0	2.5×10^{18}	1.7×10^{18}
	366 (68)	2.7	22.0±3.5	81.5±13.0	814.8	8.2×10^{25}	2.3×10^{26}
	461 (86)	3.0	24.8±3.4	82.5±11.2	825.0	5.1×10^{37}	1.4×10^{38}
	550 (102)	1.5	9.8±1.7	65.3±11.1	653.3	1.8×10^{48}	3.9×10^{48}
	638 (118)	1.5	1.3±0.8	8.3±5.0	83.3	6.3×10^{60}	1.8×10^{60}
	730 (136)	1.5	5.8±1.5	38.3±9.9	383.3	1.3×10^{73}	1.8×10^{73}

Values are mean±s.e.m. Results from at least four recipient testes.
*The number of days from initiation of culture to transplantation.
†It is assumed that 10% of transplanted stem cells can colonize the testis (Nagano et al., 1999).
‡The increase in GS or stem cell number from the first transplantation.
§(Increase in GS cell number at indicated time point)×(Stem cells/10^5 GS cells at indicated time point)/(Stem cells/10^5 GS cells at first transplantation).

embryo, ES cells and EG cells induces aberrant genomic imprinting, which can lead to morphological or functional abnormalities in embryo or offspring (Sasaki et al., 1995; Dean et al., 1998; Humpherys et al., 2001). Surprisingly, composition of the medium can also influence the imprint pattern (Doherty et al., 2000; Khosla et al., 2002; Ecker et al., 2004). The instability of these embryonic germline cells probably reflects their embryonic origin, which is susceptible to subtle changes in the maternal environment. However, our results strongly suggest that spermatogonial stem cells have sophisticated repair mechanisms to prevent transmission of genetic or epigenetic damage to the progenitors, which may be similar to the those found in postnatal stem cells in other self-renewing tissues (Cairns, 2002; Potten et al., 2002; Gilbert, 2005).

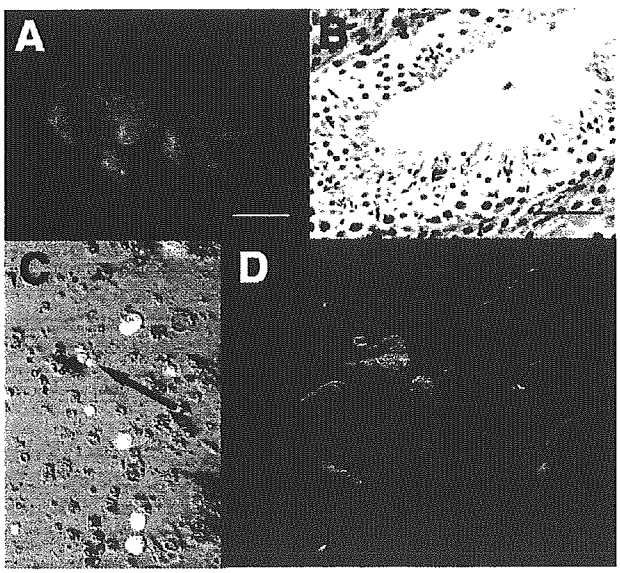

Fig. 4. Spermatogenesis and the generation of offspring from GS cells. EGFP-expressing GS cells from 24-month-old cultures were transplanted into the seminiferous tubules of infertile W recipient mice. (A) A recipient testis showing the EGFP fluorescence in GS cell-derived colonies. Green tubules represent donor GS cell colonization. (B) Histological analysis (Hematoxylin and Eosin staining) of the recipient testis showing normal-appearing spermatogenesis. (C) Round spermatid released from a recipient testis, exhibiting EGFP fluorescence (arrow). (D) Offspring resulting from the microinjection of oocytes with round spermatids, exhibiting fluorescence. Scale bar: 1 mm.

Despite their stability of spermatogonial stem cells, this study also demonstrated the shortening of telomeres during long-term culture, which suggests that these cells have limited proliferative potential. In most types of normal cells, the telomeric DNA erodes progressively with each round of cell division in the absence of telomerase activity (Blackburn, 2005). Shortened telomeres induce chromosome fusion and trigger a checkpoint that results in cell cycle arrest and apoptosis. By contrast, telomerase activity and maintenance of telomere length is associated with immortality in tumor and ES cells (Niida et al., 1998; Blackburn, 2005). As stem cells are considered to proliferate indefinitely by self-renewing division, the status of the telomeres in stem cells has been of great interest. Unlike most normal somatic cells, which do not have telomerase activity, low to moderate levels of telomerase expression have been described in adult stem cells from the skin, the gut and the hematopoietic system (Harle-Bachor et al., 1996; Kolquist et al., 1998; Allsopp et al., 2003). Telomerase plays an important role in maintaining the telomeres in male germ cells, as shown by the gradual loss of spermatogenic cells and eventual sterility in telomerase-deficient mice (Lee et al., 1998). However, our results show that telomere shortening occurs progressively during long-term culture of spermatogonial stem cells, despite the presence of telomerase activity. A similar phenomenon was also reported in hematopoietic stem cells, in which telomere shortening

Table 2. Embryo development after microinsemination

Experiment	Number of reconstituted eggs	Two cell (%)	Number of eggs transferred	Implantation sites (%)	Number of offspring (%)
1	97	74 (76.3)	73	38 (52.1)	10 (13.7)
2	10	9 (90.0)	9	5 (55.6)	2 (22.2)
3	87	70 (80.5)	48	14 (29.2)	4 (8.3)
Total	194	153 (78.9)	130	57 (43.8)	16 (12.3)

Results from three separate experiments. Embryos were cultured for 24 hours and transferred into the pseudopregnant mother. Round spermatids were used for microinsemination.

occurs after three to four rounds of serial transplantation, despite a high level of telomerase activity (Allsopp et al., 2003). These results indicate that postnatal stem cells might possess mechanisms for the regulation of telomere length that are different from those of ES cells.

Although our results show the remarkable stability of spermatogonial stem cells, our previous study has suggested that GS cells had multipotential characteristics (Kanatsu-Shinohara et al., 2004b). We reported that ES-like cells (mGS cells) appeared in the cultures during the initiation of GS cell cultures from neonatal testis cells. The origin of these mGS cells in neonatal testis cell culture is currently unknown (Kanatsu-Shinohara et al., 2004b); it is possible that they arise from a population of distinct undifferentiated pluripotent cells that persist in the testis from fetal stage. However, we previously demonstrated the direct conversion of GS cells into mGS cells in experiments using GS cells derived from p53 mutant mice that have a high frequency of teratoma (Lam and Nadeau, 2003; Kanatsu-Shinohara et al., 2004b). Based on this observation, we speculated that spermatogonial stem cells retain the ability to become multipotent cells during the early passages in vitro, an ability that may be lost during long-term cell culture (Kanatsu-Shinohara et al., 2004b). In this study, mGS cell colonies developed in 3-month-old cultures after a freeze-thaw treatment, but thereafter no other GS cells converted to mGS cells during the 2-year experimental period. This result confirms our previous observation that mGS cells appear in the early phase of neonatal testis cell culture, and also suggests that established GS cells are resistant to mGS cell conversion. Although current culture conditions support the germline potential in spermatogonial stem cells, they do not fully support the multilineage potential attributed to spermatogonial stem cells. Further studies will be necessary to determine whether mGS cells are derived from GS cells, and a special effort should be made to establish improved culture conditions that maintain the full developmental potential of spermatogonial stem cells.

Spermatogonial stem cells represent an ideal model in which to investigate the unique biology of stem cells. Spermatogonial stem cells can be transplanted between animals, genetically manipulated and cultivated under feeder-cell or serum-free conditions (Brinster and Zimmermann, 1994; Kubota et al., 2004; Kanatsu-Shinohara et al., 2005a, Kanatsu-Shinohara et al., 2005b). These advantages are not available for stem cells in other self-renewing systems. Using these techniques, spermatogonial stem cells can now be routinely expanded and subsequently examined for molecular and genetic characteristics. Future studies will determine the mechanism by which spermatogonial stem cells maintain the stable characteristics. In addition, the long-term stability of GS cells will provide a strong advantage in practical application, and may complement ES cell technology. Although the shortening telomeres suggests that spermatogonial stem cells have limited proliferative potential, it would not be a serious concern in practical application of GS cells; assuming a constant rate of telomere loss, GS cells should continue to proliferate for 34 months and achieve ~10^{120}-fold expansion before they undergo crisis. This should allow a sufficient time for in vitro genetic modification of GS cells for various purposes, including gene targeting. Thus, GS cells provide a new possibility in the study of stem cell biology and will be an attractive target of germline modification.

We thank Dr Y. Kaziro for encouragement and critical reading and Ms A. Wada for technical assistance. Financial support for this research was provided by the Ministry of Education, Culture, Sports, Science and Technology (MEXT) of Japan, and by grants from CREST and the Human Science Foundation (Japanese). This work was also supported in part by Special Coordination Funds for Promoting Science and Technology from MEXT.

References

Allsopp, R. C., Morin, G. B., Horner, J. W., DePinho, R., Harley, C. B. and Weissman, I. L. (2003). Effect of TERT over-expression on the long-term transplantation capacity of hematopoietic stem cells. *Nat. Med.* **9**, 369-371.

Blackburn, E. H. (2005). Telomeres and telomerase: their mechanisms of action and the effects of altering their functions. *FEBS Lett.* **579**, 859-862.

Brinster, R. L. and Zimmermann, J. W. (1994). Spermatogenesis following male germ-cell transplantation. *Proc. Natl. Acad. Sci. USA* **91**, 11298-11302.

Buaas, F. W., Kirsch, A. L., Sharma, M., McLean, D. J., Morris, J. L., Griswold, M. D., de Rooij, D. G. and Braun, R. E. (2004). Plzf is required in adult male germ cells for stem cell self-renewal. *Nat. Genet.* **36**, 647-652.

Cairns, J. (2002). Somatic stem cells and the kinetics of mutagenesis and carcinogenesis. *Proc. Natl. Acad. Sci. USA* **99**, 10567-10570.

Cervantes, R. B., Stringer, J. R., Shao, C., Tischfield, J. A. and Stambrook, P. J. (2002). Embryonic stem cells and somatic cells differ in mutation frequency and type. *Proc. Natl. Acad. Sci. USA* **99**, 3586-3590.

Chambers, I., Colby, D., Robertson, M., Nichols, J., Lee, S., Tweedie, S. and Smith, A. (2003). Functional expression cloning of Nanog, a pluripotency sustaining factor in embryonic stem cells. *Cell* **113**, 643-655.

Costoya, J. A., Hobbs, R. M., Barna, M., Cattoretti, G., Manova, K., Sukhwani, M., Orwig, K. E., Wolgemuth, D. J. and Pandolfi, P. P. (2004). Essential role of Plzf in maintenance of spermatogonial stem cells. *Nat. Genet.* **36**, 653-659.

de Rooij, D. G. and Russell, L. D. (2000). All you wanted to know about spermatogonia but were afraid to ask. *J. Androl.* **21**, 776-798.

Dean, W., Bowden, L., Aitchison, A., Klose, J., Moore, T., Menesses, J. J., Reik, W. and Feil, R. (1998). Altered imprinted gene methylation and expression in completely ES cell-derived mouse fetuses: association with aberrant phenotypes. *Development* **125**, 2273-2282.

Doherty, A. S., Mann, M. R. W., Tremblay, K. D., Bartolomei, M. S. and Schultz, R. M. (2000). Differential effects of culture on imprinted H19 expression in the preimplantation embryo. *Biol. Reprod.* **62**, 1526-1535.

Draper, J. S., Smiths, K., Gokhale, P., Moore, H. D., Maltby, E., Johnson,

J., Meisner, L., Zwaka, T. P., Thomson, J. A. and Andrews, P. W. (2004). Recurrent gain of chromosomes 17q and 12 in cultured human embryonic stem cells. *Nat. Biotechnol.* **22**, 53-54.

Ecker, D. J., Stein, P., Xu, Z., Williams, C. J., Kopf, G. S., Bilker, W. B., Abel, T. and Schultz, R. M. (2004). Long-term effects of culture of preimplantation mouse embryos on behavior. *Proc. Natl. Acad. Sci. USA* **101**, 1595-1600.

Evans, M. J. and Kaufman, M. H. (1981). Establishment in culture of pluripotential cells from mouse embryos. *Nature* **292**, 154-156.

Falender, A. E., Freiman, R. N., Geles, K. G., Lo, K. C., Hwang, K., Lamb, D. J., Morris, P. L., Tjian, R. and Richards, J. S. (2005). Maintenance of spermatogenesis requires TAF4b, a gonad-specific subunit of TFIID. *Genes Dev.* **19**, 794-803.

Fujiwara, Y., Komiya, T., Kawabata, H., Sato, M., Fujimoto, H., Furusawa, M. and Noce, T. (1994). Isolation of a DEAD-family protein gene that encodes a murine homolog of Drosophila vasa and its specific expression in germ cell lineage. *Proc. Natl. Acad. Sci. USA* **91**, 12258-12262.

Gilbert, G. H. (2005). Label-retaining epithelial cells in mouse mammary gland divide asymmetrically and retain their template DNA strands. *Development* **132**, 681-687.

Giuili, G., Tomljenovic, A., Labrecque, N., Oulad-Abdelghani, M., Raaaoulzadegan, M. and Cuzin, F. (2002). Murine spermatogonial stem cells: targeted transgene expression and purification in an active state. *EMBO Rep.* **3**, 753-759.

Harle-Bachor, C. and Boukamp, P. (1996). Telomerase activity in the regenerative basal layer of the epidermis in human skin and in immortal and carcinoma-derived skin keratinocytes. *Proc. Natl. Acad. Sci. USA* **93**, 6476-6481.

Humpherys, D., Eggan, K., Akutsu, H., Hochedlinger, K., Rideout III, W. M., Biniszkiewicz, D., Yanagimachi, R. and Jaenisch, R. (2001). Epigenetic instability in ES cells and cloned mice. *Science* **293**, 95-97.

Kanatsu-Shinohara, M., Ogonuki, N., Inoue, K., Ogura, A., Toyokuni, S., Honjo, T. and Shinohara, T. (2003a). Allogeneic offspring produced by male germ line stem cell transplantation into infertile mouse testis. *Biol. Reprod.* **68**, 167-173.

Kanatsu-Shinohara, M., Ogonuki, N., Inoue, K., Miki, H., Ogura, A., Toyokuni, S. and Shinohara, T. (2003b). Long-term proliferation in culture and germline transmission of mouse male germline stem cells. *Biol. Reprod.* **69**, 612-616.

Kanatsu-Shinohara, M., Ogonuki, N., Inoue, K., Ogura, A., Toyokuni, S. and Shinohara, T. (2003c). Restoration of fertility in infertile mice by transplantation of cryopreserved male germline stem cells. *Hum. Reprod.* **18**, 2660-2667.

Kanatsu-Shinohara, M., Toyokuni, S. and Shinohara, T. (2004a). CD9 is a surface marker on mouse and rat male germline stem cells. *Biol. Reprod.* **70**, 70-75.

Kanatsu-Shinohara, M., Inoue, K., Lee, J., Yoshimoto, M., Ogonuki, N., Miki, H., Baba, S., Kato, T., Kazuki, Y., Toyokuni, S. et al. (2004b). Generation of pluripotent stem cells from neonatal mouse testis. *Cell* **119**, 1001-1012.

Kanatsu-Shinohara, M., Toyokuni, S. and Shinohara, T. (2005a). Genetic selection of mouse male germline stem cells in vitro: Offspring from single stem cells. *Biol. Reprod.* **72**, 236-240.

Kanatsu-Shinohara, M., Miki, H., Inoue, K., Ogonuki, N., Toyokuni, S., Ogura, A. and Shinohara, T. (2005b). Long-term culture of mouse male germline stem cells under serum- or feeder-free conditions. *Biol. Reprod.* **72**, 985-991.

Khosla, S., Dean, W., Brown, D., Reik, W. and Feil, R. (2001). Culture of preimplantation mouse embryos affects fetal development and the expression of imprinted genes. *Biol. Reprod.* **64**, 918-926.

Kimura, Y. and Yanagimachi, R. (1995). Mouse oocytes injected with testicular spermatozoa or round spermatids can develop into normal offspring. *Development* **121**, 2397-2405.

Kolquist, K. A., Ellisen, L. W., Counter, C. M., Meyerson, M., Tan, L. K., Weinberg, R. A., Harber, D. A. and Gerald, W. L. (1998). Expression of TERT in early premalignant lesions and a subset of cells in normal tissues. *Nat. Genet.* **19**, 182-186.

Kubota, H., Avarbock, M. R. and Brinster, R. L. (2004). Growth factors essential for self-renewal and expansion of mouse spermatogonial stem cells. *Proc. Natl. Acad. Sci. USA* **101**, 16489-16494.

Labosky, P. A., Barlow, D. P. and Hogan, B. L. M. (1994). Mouse embryonic germ (EG) cell lines: transmission through the germline and differences in the methylation imprint of insulin-like growth factor 2 receptor (Igf2r) gene compared with embryonic stem (ES) cell lines. *Development* **120**, 3197-3204.

Lam, M.-Y. J. and Nadeau, J. H. (2003). Genetic control of susceptibility to spontaneous testicular germ cell tumors in mice. *Acta Pathol. Mic. Sc.* **111**, 184-191.

Lee, H.-W., Blasco, M. A., Gottlieb, G. J., Horner, II, J. W., Greider, C. W. and DePinho, R. A. (1998). Essential role of mouse telomerase in highly proliferative organs. *Nature* **392**, 569-574.

Liu, X., Wu, H., Loring, J., Hormuzdi, S., Disteche, C. M., Bornstein, P. and Jaenisch, R. (1997). Trisomy eight in ES cells is a common potential problem in gene targeting and interferes with germ line transmission. *Dev. Dyn.* **209**, 85-91.

Longo, L., Bygrave, A., Grosveld, F. G. and Pandolfi, P. P. (1997). The chromosome make-up of mouse embryonic stem cells is predictive of somatic and germ cell chimaerism. *Transgenic Res.* **6**, 321-328.

Martin, G. R. (1981). Isolation of a pluripotent cell line from early mouse embryos cultured in medium conditioned by teratocarcinoma stem cells. *Proc. Natl. Acad. Sci. USA* **78**, 7634-7638.

Matsui, Y., Zsebo, K. and Hogan, B. L. M. (1992). Derivation of pluripotential embryonic stem cells from murine primordial germ cells in culture. *Cell* **70**, 841-847.

Meistrich, M. L. and van Beek, M. E. A. B. (1993). Spermatogonial stem cells. In *Cell and Molecular Biology of the Testis* (ed. C. Desjardins and L. L. Ewing), pp. 266-295. New York: Oxford University Press.

Meng, X., Lindahl, M., Hyvönen, M. E., Parvinen, M., de Rooij, D. G., Hess, M. W., Raatikainen-Ahokas, A., Sainio, K., Rauvala, H., Lakso, M. et al. (2000). Regulation of cell fate decision of undifferentiated spermatogonia by GDNF. *Science* **287**, 1489-1493.

Mitsui, K., Tokuzawa, Y., Itoh, H., Segawa, K., Murakami, M., Takahashi, K., Maruyama, M., Maeda, M. and Yamanaka, S. (2003). The homeoprotein Nanog is required for maintenance of pluripotency in mouse epiblast and ES cells. *Cell* **113**, 631-642.

Nagano, M., Avarbock, M. R. and Brinster, R. L. (1999). Pattern and kinetics of mouse donor spermatogonial stem cell colonization in recipient testes. *Biol. Reprod.* **60**, 1429-1436.

Niida, H., Matsumoto, T., Satoh, H., Shiwa, M., Tokutake, Y., Furuichi, Y. and Shinkai, Y. (1998). Severe growth defect in mouse cells lacking the telomerase RNA component. *Nat. Genet.* **19**, 203-206.

Ogawa, T., Aréchaga, J. M., Avarbock, M. R. and Brinster, R. L. (1997). Transplantation of testis germinal cells into mouse seminiferous tubules. *Int. J. Dev. Biol.* **41**, 111-122.

Ogawa, T., Ohmura, M., Tamura, Y., Kita, K., Ohbo, K., Suda, T. and Kubota, Y. (2004). Derivation and morphological characterization of mouse spermatogonial stem cell lines. *Arch. Histol. Cytol.* **67**, 297-306.

Ohta, H., Tohda, A. and Nishimune, Y. (2003). Proliferation and differentiation of spermatogonial stem cells in the W/W^{v} mutant mouse testis. *Biol. Reprod.* **69**, 1815-1821.

Pesce, M. and Schöler, H. R. (2001). Oct-4: gatekeeper in the beginning of mammalian development. *Stem Cells* **19**, 271-278.

Potten, C. S. (1992). Cell lineages. In *Oxford Textbook of Pathology* (ed. J. O. McGee, P. G. Isaacson and N. A. Wright), pp. 43-52. Oxford: Oxford University Press.

Potten, C. S., Owen, G. and Booth, D. (2002). Intestinal stem cells protect their genome by selective segregation of template DNA strands. *J. Cell. Sci.* **115**, 2381-2388.

Resnick, J. L., Bixler, L. S., Cheng, L. and Donovan, P. J. (1992). Long-term proliferation of mouse primordial germ cells in culture. *Nature* **359**, 550-551.

Rubin, H. (2002). The disparity between human cell senescence in vitro and lifelong replication in vivo. *Nat. Biotechnol.* **20**, 675-681.

Ryu, B.-Y., Orwig, K. E., Kubota, H., Avarbock, M. R. and Brinster, R. L. (2004). Phenotypic and functional characteristics of male germline stem cells in rats. *Dev. Biol.* **274**, 158-170.

Saitou, M., Barton, S. C. and Surani, M. A. (2002). A molecular program for the specification of germ cell fate in mice. *Nature* **418**, 293-300.

Sasaki, H., Ferguson-Smith, A. C., Shum, A. S. W., Barton, S. C. and Surani, M. A. (1995). Temporal and spatial regulation of *H19* imprinting in normal and uniparental mouse embryos. *Development* **121**, 4195-4202.

Shinohara, T., Avarbock, M. R. and Brinster, R. L. (1999). β1- and α6-integrin are surface markers on mouse spermatogonial stem cells. *Proc. Natl. Acad. Sci. USA* **96**, 5504-5509.

Shinohara, T., Orwig, K. E., Avarbock, M. R. and Brinster, R. L. (2000). Spermatogonial stem cell enrichment by multiparameter selection of mouse testis cells. *Proc. Natl. Acad. Sci. USA* **97**, 8346-8351.

Shinohara, T., Orwig, K. E., Avarbock, M. R. and Brinster, R. L. (2001). Remodeling of the postnatal mouse testis is accompanied by dramatic changes in stem cell number and niche accessibility. *Proc. Natl. Acad. Sci. USA* **98**, 6186-6191.

Solter, D. and Knowles, B. B. (1978). Monoclonal antibody defining a stage-specific mouse embryonic antigen (SSEA-1). *Proc. Natl. Acad. Sci. USA* **75**, 5565-5569.

Takahashi, K., Mitsui, K. and Yamanaka, S. (2003). Role of Eras in promoting tumor-like properties in mouse embryonic stem cells. *Nature* **414**, 122-128.

Tatematsu, T., Nakayama, J., Danbara, M., Shionoya, S., Sato, H., Omine, M. and Ishikawa, F. (1996). A novel quantitative 'stretch PCR assay', that detects a dramatic increase in telomerase activity during the progression of myeloid leukemias. *Oncogene* **13**, 2265-2274.

Xiong, Z. and Laird, P. W. (1997). COBRA: a sensitive and quantitative DNA methylation assay. *Nucleic Acids Res.* **25**, 2532-2534.

Yoshida, S., Takakura, A., Ohbo, K., Abe, K., Wakabayashi, J., Yamamoto, M., Suda, T. and Nabeshima, Y. (2004). Neurogenenin3 delineates the earliest stages of spermatogenesis in the mouse testis. *Dev. Biol.* **269**, 447-458.

TECHNOLOGY REPORT

Noninvasive Visualization of Molecular Events in the Mammalian Zygote

Kazuo Yamagata,[1]* Taiga Yamazaki,[1] Misuzu Yamashita,[1] Yuki Hara,[1] Narumi Ogonuki,[2] and Atsuo Ogura[2]

[1]Graduate School of Life and Environmental Science, and Institute of Applied Biochemistry, University of Tsukuba, Tsukuba Science City, Ibaraki, Japan

[2]RIKEN Bioresource Center, Koyadai, Tsukuba Science City, Ibaraki, Japan

Received 1 April 2005; Accepted 16 July 2005

Summary: Following fertilization, a number of molecular events are triggered in the mammalian zygote. As biochemical studies using mammalian gametes and zygotes have inherent difficulties, the molecular nature of these processes is currently unclear. We have developed a method to visualize these events. In vitro transcribed mRNAs encoding for proteins fused with green fluorescent protein were microinjected into oocytes or embryos and fluorescence signals were observed. Using this technique we succeeded in obtaining images of the DNA methylation status in living mouse and rabbit embryos. Moreover, time-lapse images were acquired of spindle and nuclear formation during second meiosis and first mitosis. Importantly, the microinjected embryos developed to the normal offspring even after observation, suggesting that the technique is relatively noninvasive. Thus, our method may help elucidate the molecular aspects of fertilization and preimplantation development and, based on the real-time genetic and epigenetic status, could become a tool to select "good quality" embryos before implantation. genesis 43:71–79, 2005. © 2005 Wiley-Liss, Inc.

Key words: fertilization; one-cell zygote; preimplantation development; fluorescence imaging; DNA methylation; spindle formation

Fertilization and subsequent development are irreversible processes of the dynamic conversion of two highly specialized cells—the sperm and egg—into totipotent zygotes. They consist of sequential multistep events of sperm–egg interaction, followed by interaction between maternal and paternal genomes. Once a sperm enters the ooplasm, the oocyte, arrested at metaphase II, is activated. This triggers a number of molecular cascades, such as those involved in the reinitiation of the cell cycle and in de novo gene transcription. Moreover, recent progress using nuclear transfer (NT) has revealed that these processes are associated with a set of dynamic epigenetic changes, known as nuclear reprogramming (Fulka *et al.*, 2004), in which the sex-specific epigenetic "memories" of the gametes are erased and those of the embryo are gradually acquired. Despite their scientific interests, most molecular mechanisms in these postfertilization events remain unclear, because biochemical studies using mammalian zygotes have inherent difficulties: few cells are available at any time and there are no available cell lines. As an alternative, immunostaining of fixed zygotes has frequently been used to localize specific intracellular molecules. However, it is impossible to perform time-lapse analysis and retrospective analysis because the molecular distributions observed in fixed embryos cannot be linked directly with their development. Therefore, green fluorescent protein (GFP)-based fluorescence imaging of living oocytes and zygotes is a powerful technique to understand the molecular bases of fertilization and preimplantation development (Zernicka-Goetz and Pines, 2001). Although there are methods described for the visualization of fluorescence signals in immature and mature oocytes (Aida *et al.*, 2001; Brunet *et al.*, 1998), and in later stages of preimplantation embryos (Louvet-Vallee *et al.*, 2005; Zernicka-Goetz and Pines, 2001), there is no standardized method for long-term, noninvasive observations of mature oocytes and one-cell zygotes. In this report, we document how we improved the efficiency of translation of GFP-fusion proteins in oocytes and zygotes, optimized the conditions for microinjection, and set up imaging systems for time-lapse recording.

In mouse embryos, microinjected transgenes express enhanced GFP (EGFP) from the two-cell stage at detected levels if a strong promoter, such as β-actin (Devgan *et al.*, 2004), is used. To express fluorescent proteins in mature oocytes and one-cell zygotes effi-

This article includes Supplementary Material available via the Internet at http://www.interscience.wiley.com/jpages/1526-954X/suppmat.

*Correspondence to: Kazuo Yamagata, Graduate School of Life and Environmental Science, and Institute of Applied Biochemistry, University of Tsukuba, Tsukuba Science City, Ibaraki 305-8572, Japan.

E-mail: kazuo@agbi.tsukuba.ac.jp

Published online in Wiley InterScience (www.interscience.wiley.com).

DOI: 10.1002/gene.20158

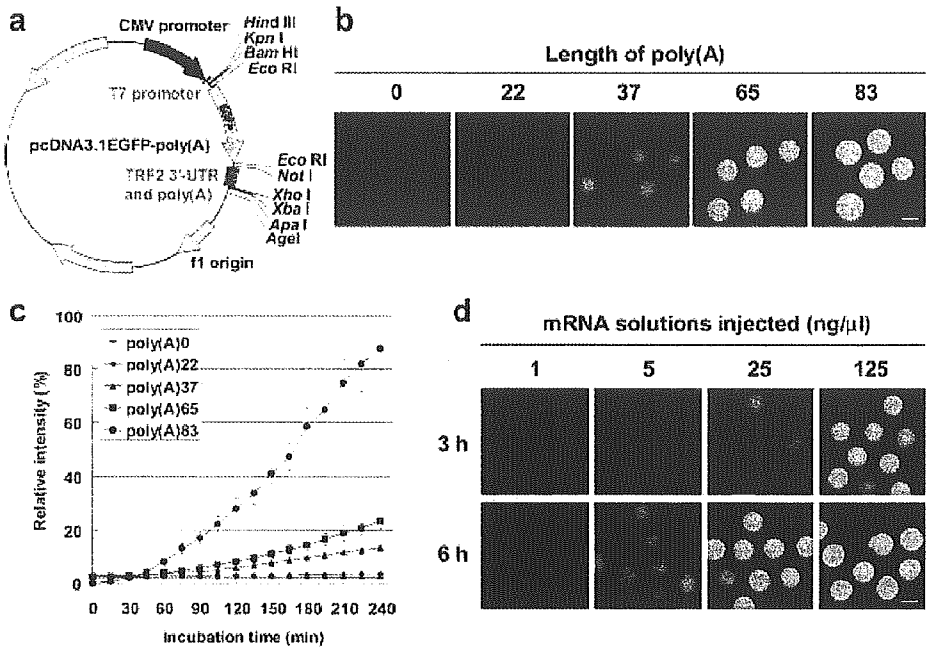

FIG. 1. Translational efficiency of the poly(A) length and amount of mRNA. **a:** Plasmid map of pcDNA3.1EGFP-poly(A). We generated a plasmid (pcDNA3.1-poly(A)) to synthesize mRNA in vitro, which is efficiently translated in oocytes and zygotes. mRNA is transcribed under the T7 promoter with a stretched poly(A) sequence downstream of and a 3′-untranslated region (UTR) derived from the mouse TRF2 gene (see Materials and Methods). As this plasmid also has a cytomegalovirus (CMV) promoter and putative poly(A) attachment signal in the 3′-UTR, encoded proteins can be expressed by transfection into various cell lines. **b,c:** EGFP mRNA (100 ng/μL) with various lengths of polyadenine (0, 22, 37, 65, or 83 bp) was injected into metaphase II oocytes. After injection the oocytes were transferred to an incubator on the microscope stage and time-lapse observation was performed under the same conditions for each mRNA. **b:** Fluorescence images of oocytes after 3 h of incubation. Scale bar = 50 μm. **c:** Intensity of fluorescence signals in oocytes. Fluorescence images of the oocyte were acquired at 15-min intervals and the intensity of whole oocytes was estimated. In the graph the vertical axis is represented as relative intensity (%) with the highest intensity of an oocyte after 240 min incubation set at 100%. To normalize the amount of mRNA injected, 50 μM TRITC-labeled dextran was coinjected and the intensity of EGFP fluorescence emission was divided by that of the TRITC. The data indicate the means ± SD of five oocytes. **d:** Increasing amounts (1, 5, 25, or 125 ng/μL of mRNA solution) of EGFP mRNA with 83-bp polyadenine were injected into metaphase II oocytes and fluorescence images were acquired after 3 h incubation. Scale bar = 50 μm.

Table 1
Development of Embryos Injected With EGFP mRNA[a]

Concentration of mRNA injected	No. of oocytes used	Percentage of surviving oocytes[b]	Percentage of embryos developed				
			2-cell	4-cell	8-cell	Morula	Blastocyst
1 mg/mL	45	80% (36/45)	97% (35/36)	94% (34/36)	86% (31/36)	36% (13/36)	3%[c] (1/36)
0.1 mg/mL	69	90% (62/69)	100% (62/62)	100% (62/62)	98% (61/62)	86% (53/62)	69% (43/62)
0.01 mg/mL	44	86% (38/44)	100% (38/38)	100% (38/38)	100% (38/38)	95% (36/38)	89% (34/38)
No injection	57	100% (57/57)	100% (57/57)	100% (57/57)	98% (56/57)	98% (56/57)	91% (52/57)

[a]Pronuclear-stage embryos were injected with various concentrations of mRNA, transferred to KSOM medium, and further cultured for 72 h.
[b]The survival rate of embryos was determined just after mRNA injection.
[c]Developmental rate of embryos injected with 1 mg/ml mRNA was significantly low ($P < 0.01$), as analyzed by Student's *t*-test.

ciently, we used the mRNA injection technique (Vassalli *et al.*, 1989), with some modifications. In the cytoplasm of metaphase II oocytes, much maternal mRNA is accumulated as translational inactive forms because of its short poly(A) length (Richter, 1999). Therefore, we designed a plasmid for in vitro transcription, which intrinsically has an extended poly(A) sequence downstream of multicloning sites (Fig. 1a). The plasmid, named pcDNA3.1EGFP-poly(A), encodes EGFP, and its mRNA can be transcribed in vitro under the regulation of the T7 promoter. To determine the optimal poly(A) length to express proteins in oocytes, we injected EGFP mRNAs with various lengths of poly(A) tails into metaphase II oocytes and estimated the fluorescent intensities at 15-min intervals during incubation (Fig. 1b,c). Although no detectable fluorescence signals were observed in mRNAs with no poly(A) and 22 adenines even after 240 min incubation, mRNA with poly(A83) yielded the highest fluorescence at all time points. Moreover, the more mRNA injected, the brighter the signal

obtained (Fig. 1d). These data indicate that fluorescence intensity depends on the length of the poly(A) tail and the amount of mRNA injected. However, an excess amount of mRNA caused developmental retardation or arrest (Table 1). When we injected HcRED (see Materials and Methods)-labeled histone H4 mRNA (more than 100 ng/μL), development was retarded, whereas the same concentration of EGFP-labeled histone H4 mRNA did not cause this (data not shown). Thus, embryo development seems to be affected by the types and amounts of fluorescent proteins microinjected. In our systems, however, the amount of fluorescent proteins could be optimized by adjusting the length of the poly(A) tails and the amount of mRNA (Fig. 1). They should therefore be optimized for each construct to permit normal development.

We next established a series of experimental procedures that consisted of mRNA injection, insemination, and observation. To observe the fluorescence signals during the transition stages of oocyte to zygote, metaphase II oocytes were first microinjected with the mRNA, incubated until fluorescence was detected, and then inseminated by in vitro fertilization (IVF) or intracytoplasmic sperm injection (ICSI) (Series 1). The imaging of late one-cell zygotes and subsequent preimplantation embryos was performed following the mRNA microinjection of pronuclear stage embryos (Series 2). Details of the microinjection and the imaging system are described in Materials and Methods and Supplementary Figures 1 and 2.

To demonstrate the usefulness of our experimental systems, we performed two pilot experiments. We first attempted to monitor DNA methylation status in living embryos. DNA methylation is a key player in epigenetic modification and genome-wide demethylation in parental DNA during preimplantation development is thought to be responsible for nuclear reprogramming (Reik *et al.*, 2001). In addition, by immunostaining with anti-5-methylcytosine antibody, paternal chromatin-specific hypomethylation has been reported in one-cell zygotes from some mammalian species including the mouse, but not in the rabbit or sheep (Beaujean *et al.*, 2004a; Mayer *et al.*, 2000). The EGFP fusion protein with partial amino acid sequence of human methyl-CpG binding protein 1 (MBD1) encoding methylcytosine binding domain and nuclear localization signal have been developed as a reporter for the localization of methylated DNA in living cells. (Fujita *et al.*, 1999). We injected the mRNA of this fusion protein, termed EGFP-MBD-NLS, into embryos

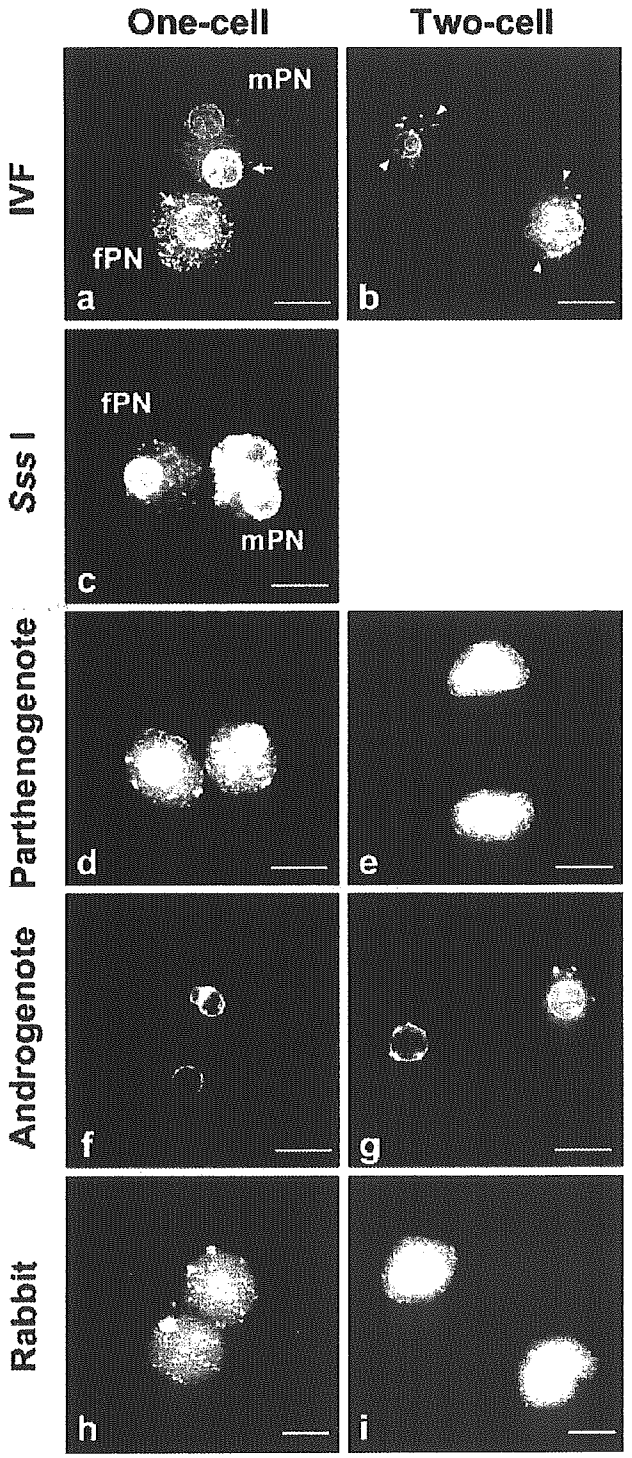

FIG. 2. DNA methylation status in living mouse and rabbit embryos. Five nanograms per microliter or 100 ng/μL of EGFP-MBD-NLS mRNA was injected into embryos from mice (**a–g**) or rabbits (**h,i**), respectively. After the injection embryos were incubated in culture media and observed periodically. One-cell stage embryos (**a,c,d,f,h**) represent the images just before prometaphase, and the two-cell images (**b,e,g,i**) are embryos 24 h after insemination. **a:** Pronuclear-stage zygote from mouse. Arrows indicate the signals around nucleoli in male and female pronuclei. **b:** Mouse two-cell stage embryo. Arrowheads indicate the boundary of male and female chromatin arrays. **c:** Zygote coinjected with *Sss* I methyltransferase mRNA. Note that intense signals were apparently observed in nucleus. **d,e:** Mouse parthenogenetic embryos. **f,g:** Mouse androgenotes. **h,i:** Rabbit embryos. mPN, male pronucleus; fPN, female pronucleus. Scale bar = 20 μm.

Table 2
Development of Embryos Injected With Fusion Protein mRNA[a]

mRNA injected	No. of oocytes injected	Percentage of surviving oocytes[b]	Percentage of embryos developed				
			2-cell	4-cell	8-cell	Morula	Blastocyst
EGFP-MBD-NLS (5 ng/μL)	45	87% (39/45)	97% (38/39)	82% (32/39)	67% (26/39)	59% (23/39)	46% (18/39)
EGFP-MBD-NLS (1 ng/μL)[c]	45	80% (36/45)	97% (35/36)	92% (33/36)	92% (33/36)	92% (33/36)	92%[e] (33/36)
EGFP-tubulin + HcRED-histone H4	75	90% (68/75)	98% (67/68)	97% (66/68)	96% (65/68)	91% (62/68)	88%[f] (60/68)
Control[d]	40	87% (35/40)	97% (34/35)	94% (33/35)	94% (33/35)	94% (33/35)	94% (33/35)

[a]Pronuclear-stage embryos were injected with mRNA, incubated for 6 h, and fluorescent images acquired by excitation at 488 nm for 200 ms five times (total 1 s). After observation, embryos were transferred to KSOM medium and further cultured for 72 h.
[b]The survival rate of embryos was determined just after mRNA injection.
[c]Fluorescence signals were also detectable at this concentration (see Suppl. Fig. 3).
[d]Control experiments were performed with TE buffer injection.
[e,f]No significant difference with control group as analyzed by Student's *t*-test.

Table 3
Full-Term Development of Embryos Injected With mRNA[a]

mRNA injected	No. of recipients	No. of transferred 2-cell embryos[b]	No. (%) of embryos implanted[c]	No. (%) of newborn mice[d]	No. (%) of transgenic pups[e]
EGFP-MBD-NLS	6	86	67 (78)	51 (76)	0 (0)
EGFP	3	37	33 (89)	28 (76)	0 (0)
Control[f]	3	36	23 (64)	22 (61)	n.d.

[a]Pronuclear-stage embryos were injected with mRNA, incubated for 6 h, and fluorescent images acquired by excitation at 488 nm for 200 ms five times (total 1 s). After observation, embryos were transferred to KSOM medium and further cultured to two-cell stage.
[b]The two-cell embryos were transferred to recipient mice.
[c,d]No significant difference between groups as analyzed by Student's *t*-test.
[e]Integration of exogenous DNA into the mouse genome was analyzed by PCR using tail tip DNA from pups (see legend of Suppl. Fig. 3).
[f]Control experiments were performed with TE buffer injection.
n.d. = not determined.

from mouse and rabbit and observed them using fluorescence microscopy (Series 2 experiment, Fig. 2). In late one-cell zygote, we observed ring-like signals around the nucleoli of both male and female pronuclei in mice. Interestingly, multiple point signals were observed only in the female pronucleus (Fig. 2a). At the two-cell stage, both nuclei showed a highly compartmentalized localization of point signals, possibly reflecting differences between parental genomes (Fig. 2b). The zygotes coinjected with mRNA encoding *Sss* I, CpG methyltransferase, showed hypermethylated foci in pronuclei (Fig. 2c), suggesting that EGFP-MBD-NLS protein correctly bind to methylated DNA in the embryos. Next, we assayed the DNA methylation status in parthenogenetic and androgenetic embryos. The asymmetric signal pattern between male and female chromatin was also seen in both types of embryos. In parthenogenotes, both pronuclei have many punctate signals, whereas signals were detected only around the nucleoli in androgenotes (Fig. 2d,f). Moreover, unlike in normal embryos (Fig. 2b), compartmentalized patterns were not observed in either two-cell embryos (Fig. 2e,g). These data clearly indicate that the difference in methylation status signal between male and female chromatin depends on the origin of nuclei—the sperm and egg. Unlike in the mouse, this asymmetry was not observed in rabbit pronuclear or two-cell embryos (Fig. 2 h,i), as reported (Beaujean *et al.*, 2004a). It should be noted that the pronuclear stage embryos, observed under a fluorescence microscope, could develop to the blastocyst stage (Table 2) and to normal offspring (Table 3; Suppl. Fig. 3). Thus, DNA methylation status can be visualized in living embryos and they can continue to develop even after observation, suggesting that the retrospective analysis is possible by our experimental systems.

We next tried to acquire time-lapse images of nuclear and spindle formations during second meiosis and first mitosis using the combination of α-tubulin fused with EGFP and histone H4 fused with HcRED. When a mixed solution of 10 ng/μL of each mRNA was injected into pronuclear stage embryos (Series 2), they developed normally to the blastocyst stage (Fig. 3; Table 2). The signals of EGFP-tubulin were continuously detectable until the blastocyst stage, whereas those of HcRED-histone H4 were mislocated in the cytosol and gradually disappeared after the four-cell stage (Fig. 3). This indicates that mRNA and/or protein stability in embryos vary between these fusion proteins. When we performed the Series 1 experiments, a barrel-shaped spindle was clearly observed in metaphase II oocytes (Fig. 3), spindle fibers were extended, and cytoplasmic asters appeared in oocytes treated with taxol, an inhibitor of tubulin depolymerization (Fig. 3 and Suppl. Movie 1). After ICSI, we performed time-lapse observations of the second meiotic

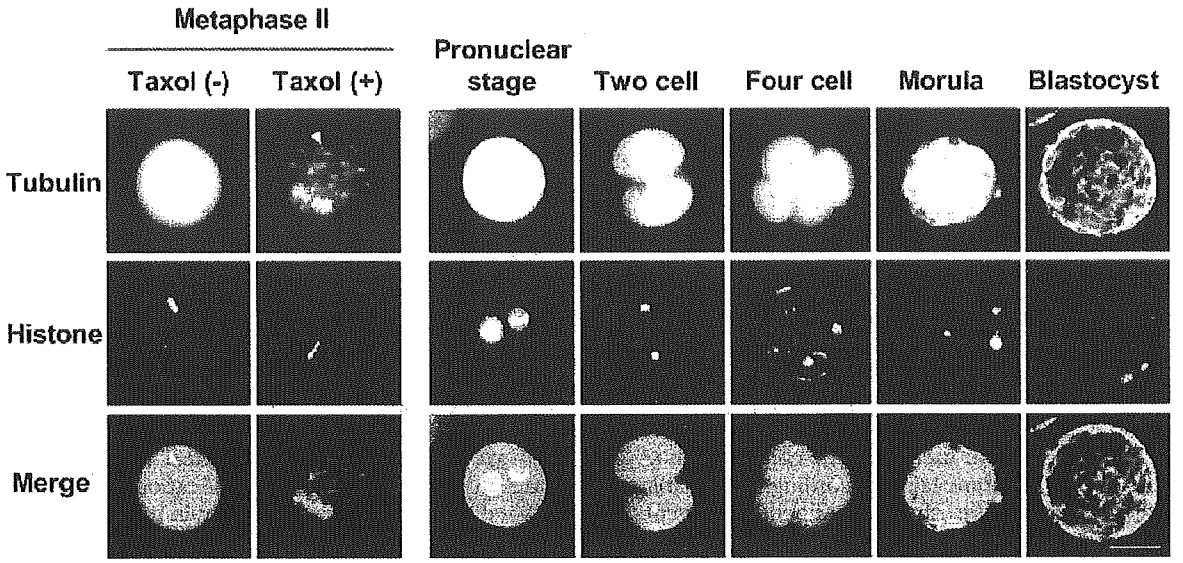

FIG. 3. Embryos coinjected with EGFP-tubulin and histone H4-HcRED mRNAs. A mixture of 10 ng/μL of each EGFP-tubulin (tubulin, green) and histone H4-HcRED (histone, red) mRNA was microinjected into metaphase II stage oocytes or pronuclear stage embryos. After injection, each stage of embryo was observed. Metaphase II oocytes were incubated for 30 min in the presence (+) or absence (–) of 10 ng/μL of taxol. The arrowhead indicates that cytoplasmic asters appeared in metaphase II oocytes following taxol treatment. Scale bar = 50 μm.

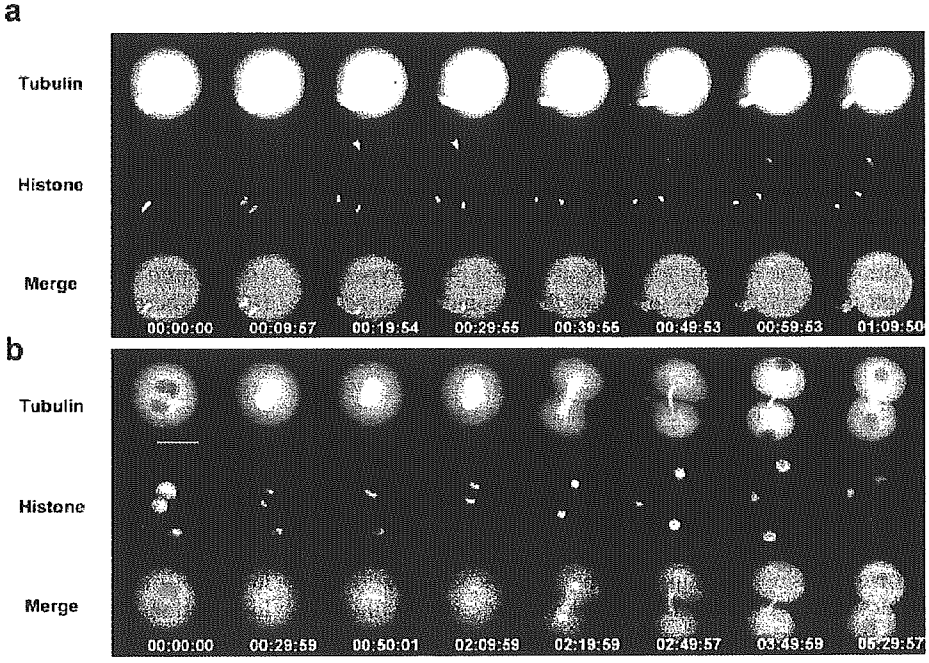

FIG. 4. Time-lapse imaging of second meiosis and first mitosis of embryo injected with EGFP-tubulin and histone H4-HcRED mRNAs. **a:** Metaphase II oocytes were injected with EGFP-tubulin (tubulin, green) and histone H4-HcRED (histone, red) mRNAs and incubated for 3 h. Just after ICSI, oocytes were transferred to Hepes-TYH medium in an incubator equipped with a microscope, and fluorescence images were acquired at 10-min intervals. Arrowheads indicate the decondensing sperm nucleus. Note that maternal histone H4 starts to be assembled in decondensing sperm nucleus and accumulates gradually during recondensation. **b:** Pronuclear stage embryos were prepared by IVF, injected with mRNAs, and observed at 10-min intervals. Scale bar = 50 μm.

division (Fig. 4a and Suppl. Movie 2). The metaphase-anaphase transition occurred about 10 min after ICSI. HcRED-histone H4, considered a maternally stored histone, started to assemble on the decondensing sperm nucleus after 20–30 min of incubation. For a time-lapse observation of first mitosis, Series 2 experiments were performed (Fig. 4b and Suppl. Movie 3). In a pronuclear stage embryo, weak signals of EGFP-tubulin were observed around the male and female pronuclei and the mitotic spindle formed just after nuclear envelope breakdown. At about 2 h after spindle formation, the first cleavage plane appeared, perpendicular to the orientation of the mitotic spindle. Interestingly, after cleavage the two nuclei moved to the periphery of the blastomeres and then returned to their central positions.

Using live-cell imaging we were able to identify the localization of target molecules in more native conditions compared with other more complicated immunos-

taining procedures using fixation and permeabilization. In addition to such procedures, the immunostaining with anti-5-methylcytosine antibody requires acid (HCl) treatment of the cells to allow the antibody to enter the chromatin. This could be damaging. On the other hand, using EGFP-MBD-NLS (Fig. 2), we observed fine-resolution localizations for methylated DNA—ring-like signals around the nucleoli and punctate signals in the female pronucleus—which have not been reported previously. Moreover, unlike the "snapshot" images, serial acquisition of images also provides new insights into fertilization and preimplantation development, which consist of many sequential events. In contrast to previous methods (Brunet *et al.*, 1998; Zernicka-Goetz and Pines, 2001), the exogenous proteins can be rapidly translated at detectable levels even in the metaphase II oocytes and one-cell zygotes in our methods. The combination of this advantage and the time-lapse recording will enables us to further investigate the time-dependent events in postfertilization.

In addition, the most important advantage of our live-cell imaging technique using embryos is that they continue to develop even after observation (Tables 2, 3 and Suppl. Fig. 3), indicating that the combination of acquiring embryo images and continuous embryo culture make retrospective analysis possible. The application of this advantage to embryos with some defects in embryogenesis will provide more information. For instance, there have been successes in cloning various mammalian species by NT (Wilmut *et al.*, 2002). However, most such embryos show developmental defects or arrest. If the embryos mature to adults they often exhibit impaired phenotypes such as oversized placentae (Wakayama *et al.*, 1998), immunological defects (Ogonuki *et al.*, 2002), and obesity (Tamashiro *et al.*, 2002). Although the reasons for these abnormal phenotypes are still unclear, the early stages of development, especially the one-cell zygote stage, could be the major step of genomic reprogramming for normal development (Fulka *et al.*, 2004). Indeed, NT embryos exhibit some aberrations in the DNA methylation status at the one-cell and two-cell stages (Beaujean *et al.*, 2004b; Dean *et al.*, 2001). Moreover, the behavior of microtubule-organizing centers in reconstructed oocytes is also important for the success of NT procedures (Miki *et al.*, 2004; Simerly *et al.*, 2003). However, as such observations are performed using immunostaining that needs fixation of oocytes, it is impossible to link the cytological findings of individual oocytes to specific phenotypes in clones. If retrospective analysis can be performed on NT embryos using this imaging technique, it might clarify why they develop abnormally. Moreover, it may help us understand the molecular mechanisms of genomic reprogramming.

As described above, living-embryo imaging has many benefits to study molecular events in postfertilization. When combined with other techniques, such as fluorescent resonance energy transfer (FRET), photobleaching, or photoactivation, we may be able to clarify protein interactions and molecular kinetics even in living mammalian embryos. Moreover, as we used mRNA injection, but not transgenesis (Table 3 and Suppl. Fig. 3), this imaging technique is applicable to other species in which the integration of transgenes is difficult, such as many domestic animals. We believe that our imaging technique will thus serve as a useful tool in the selection of "good quality" mammalian embryos before implantation in both experimental and animal production settings.

MATERIALS AND METHODS

Plasmid Construction

To obtain DNA fragments with variously sized poly(A) tails, we performed the poly(A) test (PAT) assay (Salles and Strickland, 1995) with modifications. Total RNA was isolated from the testes of ddY strain mice, ligated with a 32-mer RNA oligonucleotide adaptor (5′-UACGCAUCAUACGCUGUGGCGUACCUUGUA-3′) at the 3′ end, and reverse-transcribed using AMV reverse transcriptase XL (Takara Bio, Shiga, Japan) using the primer PAT1 (5′-ACAAGGTACGCCACAGCGTATG-3′). The synthesized first-strand cDNAs were subjected to polymerase chain reaction (PCR) amplification using the PAT1 primer and an oligonucleotide specific for the gene for mouse TBP-related factor 2 (TRF2) (5′-GGAATTCCAGTTGGAGCTAATGTGT-3′). The resulting DNA was then further amplified by nested PCR using a set of nested primers (5′-TATGTCGACTATGGGCACCAAAGAACCTG-3′) and (5′-GGCTCGAGGTACGCCACAGCGTATGATG-3′), digested with *Sal* I and *Xho* I, and subjected to polyacrylamide gel electrophoresis. The resulting fragments, appearing as a smear on the gel, were extracted as various sizes and ligated into the *Xho* I site of the pcDNA3.1/Myc-His+A vector (Invitrogen, La Jolla, CA). The lengths of poly(A) inserted were determined by sequencing.

To generate pcDNA3.1EGFP-poly(A) plasmids, cDNA encoding EGFP was ligated to the *Eco*RI site of the above pcDNA3.1-poly(A) vectors. The fusion constructs, EGFP-tubulin, EGFP-MBD-NLS, and histone H4-HcRED, were produced as described (Fujita *et al.*, 1999; Kimura and Cook, 2001; Rusan *et al.*, 2001). To isolate the cDNA fragments encoding the full length of mouse α-tubulin, histone H4, and a partial amino acid sequence containing the methylcytosine-binding domain and nuclear localization signal of human MBD1, we performed PCR amplification, using first-strand cDNA from mouse testis (tubulin and histone H4) and HeLa cells (MBD1) as templates, respectively, and the following primer sets: (5′-TTAGATCTCGGGTGCGTGAGTGCATCTCCATCCACGTT-3′) and (5′-AAGCGGCCGCTTAGTACTCCTCTCCTTCTTCCTC-3′); (5′-TGAATTCGCCACCATGTCAGGACGAGGAAAAGG-3′) and (5′-AGAATTCAAGCTTGAGCTCGAGATCGCCGCCGAAGCCGTACAGAG-3′); (5′-CCAAGCTTCATGGCTGAGGACTGGCTGGAC-3′) and (5′-AAGCGGCCGCTTACGGGGCCTCCTTCCTGACCT-3′). Amplified fragments were coinserted with EGFP or HcRED (far-red fluorescent pro-

tein derived from *Heteractis crispa*; BD Biosciences ClonTech, Palo Alto, CA) fragments to the *Eco*RI and *Not* I sites of the pcDNA3.1-poly(A) vector with 83-bp polyadenine. These fusion constructs yielded the linker peptides, SGLRSRV (EGFP-tubulin), DLELKLRILQSTVPRARDPPVAT (histone H4-HcRED), and SGRTQISSSSF (EGFP-MBD-NLS), between the target and fluorescent proteins.

Full-length *Sss* I methyltransferase gene was amplified by PCR of lyophilized powder of *Spiroplasma monobiae* (American Type Culture Collection, Rockville, MD) as a template using a primer set (5′-AAGGTACCCCCAGCAAAGTAGAAAATAAA-3′) and (5′-TTGAATTCCTGCAGATTGACATGTAT-3′). Wildtype *Sss* I have four amber mutations at amino acids 43, 83, 165, and 203. To rescue enzymatic activity in mammalian cells, we convert these amber mutations into tryptophan. Four cycles of site-direct mutagenesis were performed using following four sets of oligonucleotides (5′-GCTTGCTGAATGGTATGTTCCTGC-3′) and (5′-GCAGGAACATACCATTCAGCAAGC-3′), (5′-CACTATCTTGGAACTCAAAAAATCC-3′) and (5′-GGATTTTTTGAGTTCCAAGATAGTG-3′), (5′-GGTCTCTTATGGGAAATTGAAAGAGC-3′) and (5′-GCTCTTTCAATTTCCCATAAGAGACC-3′), and (5′-CTAAATCAATGGAAGCAAAAATTAG-3′) and (5′-CTAATTTTTGCTTCCATTGATTTAG-3′). The resulting plasmid was introduced into DH10B for further cloning. To localize the *Sss* I protein to nuclei of zygotes, Gal4 binding domain (GAL4BD) polypeptide was fused. The DNA fragment encoding GAL4BD was PCR-amplified using pGBT9 plasmid (BD Biosciences ClonTech) as a template. PCR reactions were performed using a set of primers (5′-AAGAATTCGCCACCATGAAGCTACTGTCTTCT-3′) and (5′-TTGGTACCGGGGAACTCGGGCGATACAGTCAACTG-3′). The DNA fragments encoding *Sss* I and GAL4BD were digested with *Eco* RI and *Kpn* I, then coinserted into the *Eco* RI site of pcDNA3.1-poly(A).

Synthesis of mRNA In Vitro

After the linearization of fusion constructs at the *Xba* I or *Xho* I site, in vitro mRNA syntheses were performed using RiboMAX Large Scale RNA Production Systems-T7 (Promega, Madison, WI), according to the manufacturer's protocol. For efficient translation in embryos, Ribo m7G Cap Analog (Invitrogen) was added to the reaction mixture. To circumvent the integration of template DNA into the embryo genome, reaction mixtures were treated with DNase I. Synthesized RNAs were treated with phenol-chloroform followed by ethanol precipitation. After dissolution in distilled water, mRNAs were subject to gel filtration using a MicroSpinTM G-25 column (Amersham Biosciences, Piscataway, NJ) to remove unreacted substrates and stored at -80°C until use.

Gamete Collection, Insemination, and Embryo Culture

Female ICR strain mice (7–12 weeks old; Japan SLC, Shizuoka, Japan) were superovulated by intraperitoneal injections of 7.5 IU pregnant mare serum gonadotrophin (PMSG) and 7.5 IU human chorionic gonadotrophin (hCG) (Teikoku Zoki, Tokyo, Japan) at 48-h intervals. Cumulus-intact oocytes were recovered 13–15 h after hCG injection and placed in a modified Krebs-Ringer bicarbonate solution (TYH medium) containing glucose, sodium pyruvate, bovine serum albumin, and antibiotics (Toyoda *et al.*, 1971). Cauda epididymal sperm suspensions from ICR males (Japan SLC) were collected in 0.2-mL drops of TYH medium and capacitated by incubation for 2 h at 37°C under 5% CO_2 in air. To obtain pronuclear stage embryos, cumulus-intact oocytes were inseminated with capacitated sperm (75 sperm/μL) and incubated for 6–8 h. After injection with mRNA, embryos were cultured in potassium simplex optimized medium (KSOM) (Lawitts and Biggers, 1993) at 37°C under 5% CO_2 in air.

Metaphase II stage oocytes were prepared by the short incubation of cumulus-intact oocytes in TYH containing hyaluronidase (Type-IS, 150 units/mL, Sigma, St. Louis, MO). To facilitate the entry of sperm into these oocytes, a large hole (30–50 μm) was made in the zona pellucida by piezo-driven manipulator (Primetech, Ibaraki, Japan, Suppl. Fig. 1) before mRNA injection. After incubation in TYH medium, mRNA-injected metaphase II oocytes were inseminated with capacitated sperm (400 sperm/μL) or by ICSI (Kimura and Yanagimachi, 1995).

Mature female Japanese white rabbits (age 3–5 months, Kitayama Labs, Nagano, Japan) were given subcutaneous injections of 75 IU FSH (Fertinorm P, Serono Japan, Tokyo, Japan) dissolved in glycerol, followed by an intravenous injection of 100 IU hCG (Teikoku Zoki) 48 h later. Immediately after hCG injection, females were artificially inseminated with semen collected from a male Japanese white rabbit using an artificial vagina. At 15 h after insemination, in vivo fertilized oocytes were collected by flushing the oviducts with Hepes-buffered RD medium consisting of equal parts of RPMI 1640 and low-glucose Dulbecco's modified Eagle medium (Chesne *et al.*, 2002). Cumulus cells were removed by hyaluronidase treatment and mechanical pipetting. After mRNA injection, fertilized oocytes were cultured in RD medium in a humidified atmosphere of 5% CO_2 in air at 38.5°C until observation.

For the preparation of diploid parthenogenetic embryos, unfertilized oocytes were activated by treatment with 2.5 mM $SrCl_2$ in Ca^{2+}-free CZB medium (Lawitts and Biggers, 1993) containing 5 μg/mL cytochalasin B for 20 min, followed by an additional 6-h incubation in KSOM containing 5 μg/mL cytochalasin B to prevent extrusion of the polar bodies from the oocytes. The diploid androgenetic embryos were prepared by dispermic fertilization of enucleated metaphase II oocytes, as previously reported (Kono *et al.*, 1993). Briefly, the oocytes were transferred to CZB medium buffered by Hepes (20 mM) at pH 7.4 containing 7.5 μg/mL cytochalasin B and the metaphase II chromosomes were aspirated by piezo-driven pipette. The zona pellucida were partially dissected by repetitive piezo pulses and the enucleated

oocytes were inseminated with sperm as described above. After the mRNA injection at pronuclear stage, the parthenogenotes and androgenotes were transferred to KSOM and further incubated to late one-cell zygote stage or two-cell stage.

Microinjection of mRNA

Each synthesized mRNA was diluted to an appropriate concentration using TE buffer (10 mM Tris/HCl, pH 8.0, and 0.1 mM EDTA), heated at 65°C for 3 min for denaturation, and placed on ice until microinjection. Metaphase II stage oocytes were transferred to TYH medium buffered by Hepes (20 mM) at pH 7.4 and injected with mRNA using a piezo manipulator with a narrow glass pipette (3–5 μm diameter; Suppl. Fig. 1). Once mRNA solution had been sucked into the pipette, piezo pulses were applied to oocytes placed in separate drops to break the zona and plasma membrane. A few picoliters of solution was introduced into the oocytes and the pipette was removed gently.

For injection into pronuclear stage embryos, a Femto-Jet microinjector (Eppendorf, Hamburg, Germany) was used. The pipette was filled with 1–2 μL of mRNA solution and a few picoliters was injected into the cytosol of pronuclear stage embryos placed in the above Hepes-TYH medium (Suppl. Fig. 1).

In fertilized rabbit eggs, mRNA solution was injected into the cytosol using a piezo manipulator.

Image Acquisition and Processing

The microscopic system for the imaging of living embryos is summarized in Supplementary Figure 2. To reduce cell damage, we usually used a fluorescence microscope, because high-resolution images can be obtained by shorter exposure than with a laser scanning confocal microscope. To detect weak signals with short exposure times (usually 10–1000 ms), a highly sensitive CCD camera (Spot RT SE18 with IR filter; Diagnostic Instruments, Sterling Heights, MI) was attached to a fluorescence microscope (IX-70, Olympus, Tokyo, Japan). Unlike layers of cultured cells, the mouse oocyte is thick (about 100 μm diameter) and three-dimensionally complex. We therefore selected an objective lens with an iris to gain focal depth and a series of vertical sections (about 1–10 μm interval between sections) was captured using a Z-axis motor (Mac5000, Ludl Electric Products, Hawthorne, NY).

To acquire the images, oocytes or embryos were transferred to Hepes-TYH medium or FHM (Lawitts and Biggers, 1993) (minus phenol red) in a 3.5-cm glass-bottomed dish (Matsunami Trading, Tokyo, Japan), and the dish was placed in an incubator (MI-IBC-IF, Olympus) on the microscope stage. In some cases, oocytes were held using a manipulator with a blunt pipette.

Images were then processed by deconvolution programs using MetaMorph v. 6.2r2 (Universal Imaging, West Chester, PA) and/or AutoDeblur version 9.1.2 (AutoQuant, Watervliet, NY) software and stacked to acquire one picture. For time-lapse observation, images of embryos were automatically acquired using the Multi-dimension program of MetaMorph.

ACKNOWLEDGMENTS

We thank Masatoshi Egawa for imaging assistance and members of Dr. Tadashi Baba's lab for critical reading of the article and useful discussions.

LITERATURE CITED

Aida T, Oda S, Awaji T, Yoshida K, Miyazaki S. 2001. Expression of a green fluorescent protein variant in mouse oocytes by injection of RNA with an added long poly(A) tail. Mol Hum Reprod 7:1039–1046.

Beaujean N, Hartshorne G, Cavilla J, Taylor J, Gardner J, Wilmut I, Meehan R, Young L. 2004a. Non-conservation of mammalian preimplantation methylation dynamics. Curr Biol 14:R266–267.

Beaujean N, Taylor J, Gardner J, Wilmut I, Meehan R, Young L. 2004b. Effect of limited DNA methylation reprogramming in the normal sheep embryo on somatic cell nuclear transfer. Biol Reprod 71: 185–193.

Brunet S, Polanski Z, Verlhac MH, Kubiak JZ, Maro B. 1998. Bipolar meiotic spindle formation without chromatin. Curr Biol 8:1231–1234.

Chesne P, Adenot PG, Viglietta C, Baratte M, Boulanger L, Renard JP. 2002. Cloned rabbits produced by nuclear transfer from adult somatic cells. Nat Biotechnol 20:366–369.

Dean W, Santos F, Stojkovic M, Zakhartchenko V, Walter J, Wolf E, Reik W. 2001. Conservation of methylation reprogramming in mammalian development: aberrant reprogramming in cloned embryos. Proc Natl Acad Sci U S A 98:13734–13738.

Devgan V, Rao MR, Seshagiri PB. 2004. Impact of embryonic expression of enhanced green fluorescent protein on early mouse development. Biochem Biophys Res Commun 313:1030–1036.

Fujita N, Takebayashi S, Okumura K, Kudo S, Chiba T, Saya H, Nakao M. 1999. Methylation-mediated transcriptional silencing in euchromatin by methyl-CpG binding protein MBD1 isoforms. Mol Cell Biol 19:6415–6426.

Fulka J Jr, Miyashita N, Nagai T, Ogura A. 2004. Do cloned mammals skip a reprogramming step? Nat Biotechnol 22:25–26.

Kimura H, Cook PR. 2001. Kinetics of core histones in living human cells: little exchange of H3 and H4 and some rapid exchange of H2B. J Cell Biol 153:1341–1353.

Kimura Y, Yanagimachi R. 1995. Intracytoplasmic sperm injection in the mouse. Biol Reprod 52:709–720.

Kono T, Sotomaru Y, Sato Y, Nakahara T. 1993. Development of androgenetic mouse embryos produced by in vitro fertilization of enucleated oocytes. Mol Reprod Dev 34:43–46.

Lawitts JA, Biggers JD. 1993. Culture of preimplantation embryos. In: Wassarman PM, DePamphilis ML, editors. Guide to techniques in mouse development. New York: Academic Press. p 153–164.

Louvet-Vallee S, Vinot S, Maro B. 2005. Mitotic spindles and cleavage planes are oriented randomly in the two-cell mouse embryo. Curr Biol 15:464–469.

Mayer W, Niveleau A, Walter J, Fundele R, Haaf T. 2000. Demethylation of the zygotic paternal genome. Nature 403:501–502.

Miki H, Inoue K, Ogonuki N, Mochida K, Nagashima H, Baba T, Ogura A. 2004. Cytoplasmic asters are required for progression past the first cell cycle in cloned mouse embryos. Biol Reprod 71:2022–2028.

Ogonuki N, Inoue K, Yamamoto Y, Noguchi Y, Tanemura K, Suzuki O, Nakayama H, Doi K, Ohtomo Y, Satoh M, Nishida A, Ogura A. 2002. Early death of mice cloned from somatic cells. Nat Genet 30:253–254.

Reik W, Dean W, Walter J. 2001. Epigenetic reprogramming in mammalian development. Science 293:1089–1093.

Richter JD. 1999. Cytoplasmic polyadenylation in development and beyond. Microbiol Mol Biol Rev 63:446–456.

Rusan NM, Fagerstrom CJ, Yvon AM, Wadsworth P. 2001. Cell cycle-dependent changes in microtubule dynamics in living cells expressing green fluorescent protein-alpha tubulin. Mol Biol Cell 12:971–980.

Salles FJ, Strickland S. 1995. Rapid and sensitive analysis of mRNA polyadenylation states by PCR. PCR Methods Appl 4:317–321.

Simerly C, Dominko T, Navara C, Payne C, Capuano S, Gosman G, Chong KY, Takahashi D, Chace C, Compton D, Hewitson L, Schatten G. 2003. Molecular correlates of primate nuclear transfer failures. Science 300:297.

Tamashiro KL, Wakayama T, Akutsu H, Yamazaki Y, Lachey JL, Wortman MD, Seeley RJ, D'Alessio DA, Woods SC, Yanagimachi R, Sakai RR. 2002. Cloned mice have an obese phenotype not transmitted to their offspring. Nat Med 8:262–267.

Toyoda Y, Yokoyama M, Hoshi T. 1971. Studies on the fertilization of mouse egg in vitro. Jpn J Anim Reprod 16:147–151.

Vassalli JD, Huarte J, Belin D, Gubler P, Vassalli A, O'Connell ML, Parton LA, Rickles RJ, Strickland S. 1989. Regulated polyadenylation controls mRNA translation during meiotic maturation of mouse oocytes. Genes Dev 3:2163–2171.

Wakayama T, Perry AC, Zuccotti M, Johnson KR, Yanagimachi R. 1998. Full-term development of mice from enucleated oocytes injected with cumulus cell nuclei. Nature 394:369–374.

Wilmut I, Beaujean N, de Sousa PA, Dinnyes A, King TJ, Paterson LA, Wells DN, Young LE. 2002. Somatic cell nuclear transfer. Nature 419:583–586.

Zernicka-Goetz M, Pines J. 2001. Use of green fluorescent protein in mouse embryos. Methods 24:55–60.

BIOLOGY OF REPRODUCTION 73, 1302–1311 (2005)
Published online before print 24 August 2005.
DOI 10.1095/biolreprod.105.044958

Variation in Gene Expression and Aberrantly Regulated Chromosome Regions in Cloned Mice[1]

Takashi Kohda,[3,4] Kimiko Inoue,[4,5] Narumi Ogonuki,[5] Hiromi Miki,[5] Mie Naruse,[3] Tomoko Kaneko-Ishino,[4,6] Atsuo Ogura,[4,5] and Fumitoshi Ishino[2,3,4]

Department of Epigenetics,[3] Medical Research Institute, Tokyo Medical and Dental University, Chiyoda-ku, Tokyo 101-0062, Japan
CREST,[4] Japan Science and Technology Agency (JST), Kawaguchi, Saitama 332-0011, Japan
BioResource Center,[5] RIKEN, Tsukuba, Ibaraki 305-0074, Japan
School of Health Sciences,[6] Tokai University, Bohseidai, Isehara, Kanagawa 259-1193, Japan

ABSTRACT

DNA microarray analysis was used to determine the precise genome-wide gene expression profiles of somatic cloned mice derived from Sertoli and cumulus cells. It demonstrated unexpectedly large epigenetic diversity in neonatal cloned mice, despite their normal appearance and genetic identity. In three neonatal tissues of the cloned mice, the expression of 9–40% of the genes examined was more than two times higher or lower in donor cell-dependent or -independent manners compared with normal controls. Relatively few (0.4–4%) of the genes exhibited up- or downregulation in the same manner in both types of clone. A cluster analysis of the variation in gene expression led to the identification of several chromosome regions in which gene expression was aberrantly controlled in the somatic clones. These results provide a more complete understanding of how somatic clones differ from each other and from normal individuals produced by sexual reproduction and indicate the significant difficulties that face the application of somatic cloning in regenerative medicine.

cumulus cells, developmental biology, gene regulation, Sertoli cells

INTRODUCTION

Animals cloned from somatic cells have attracted a great deal of attention due to their peculiar manner of reproduction. The somatic nuclear cloning technique itself has also had a major impact on human society because nuclear-transferred embryonic stem (ES) cells are expected to be the material best suited for therapeutic cloning. However, one must still ask: What exactly are somatic clones? Does somatic cloning produce animals and tissues identical to those of the nucleus donor animals? Unlike ES cell-derived clones, which have high rates of neonatal abnormalities [1–3], we and others have previously reported that the majority of term pups cloned from somatic cells using nuclear transfer appeared healthy on delivery, gained active movement rapidly, and grew into fertile adults, despite the low success rate due to high embryonal lethality, particularly at early postimplantation stages [4–7]. Abnormal enlarged placentas are commonly observed in both ES and somatic clones and there have been many reports on their abnormal epigenetic status, such as aberrant gene expression [6, 8–11] and DNA methylation [12]. However, it has been reported that a relatively small number of genes exhibit abnormal expression in the livers of neonatal clones derived from cumulus and ES cells compared with the number of genes expressed abnormally in the corresponding placentas of clones [8]. Recently, the long-term health consequences of somatic clones, such as obesity [13], short life span, and immune-system anomalies [14], have been reported. These results suggest that broad effects also occur in neonatal or adult somatic clones, in addition to the commonly observed enlarged placentas. Here, we present detailed gene expression data from somatically cloned mice to further understanding of their biology, a necessary step before these techniques can be applied to regenerative medicine.

MATERIALS AND METHODS

Production of Cloned Mice

Cloning by nuclear transfer was performed according to the method developed by Wakayama et al. [4], with slight modification [5]. Immature Sertoli and cumulus cells were collected from newborn male (0–8 days after birth) and mature female (2–3 mo old) C57BL/6 × DBA/2 F1 (BDF1) mice, respectively, and used as nucleus donor cells. Cloned pups were obtained from the recipients at term (Day 19.5) by cesarean section. All control mice were genetically identical to the somatic cell clones, e.g., BDF1. As the majority (95% and 82% of immature Sertoli clones and cumulus clones, respectively) of term pups appeared healthy on delivery and rapidly gained active movement under our experimental conditions, we did not select individuals but instead used all of the eight pups that we obtained. After confirmation of the start of respiration at the time of cesarean section, we killed the pups and collected tissues and organs. The control neonates were produced by in vitro fertilization and also recovered by cesarean section. All samples from cesarean section were immediately frozen and stored in liquid nitrogen until use. All procedures described here were reviewed and approved by the Animal Experimentation Committee at RIKEN and were performed in accordance with the RIKEN Guiding Principles for the Care and Use of Laboratory Animals.

DNA Microarray Experiments

The CodeLink system (Amersham Biosciences) was used to determine and compare the expression levels of 10012 genes (UniSet mouse I) in the neonatal tissues of four Sertoli cell-derived clones, four cumulus cell-derived clones, and four normal controls (two males and two females each). Total RNA was purified using Isogen (Nippon Gene). The cRNA preparation and CodeLink hybridization were conducted according to the manufacturers' protocols. The expression levels of the different genes were assessed using GenePix Pro

[1]Supported by grants from CREST, the research program of the Japan Science and Technology Agency (JST), the Uehara Memorial Science Foundation, the Ministries of Health, Labour, and Welfare for Child Health and Development (14-C) and Education, Culture, Sports, Science and Technology of Japan.
[2]Correspondence: Fumitoshi Ishino, Department of Epigenetics, Medical Research Institute, Tokyo Medical and Dental University, 2–3–10 Kanda-surugadai, Chiyoda-ku, Tokyo 101-0062, Japan.
FAX: 81 3 5280 8073; e-mail: fishino.epgn@mri.tmd.ac.jp

Received: 27 June 2005
First decision: 4 August 2005
Accepted: 22 August 2005

ISSN: 0006-3363. http://www.biolreprod.org

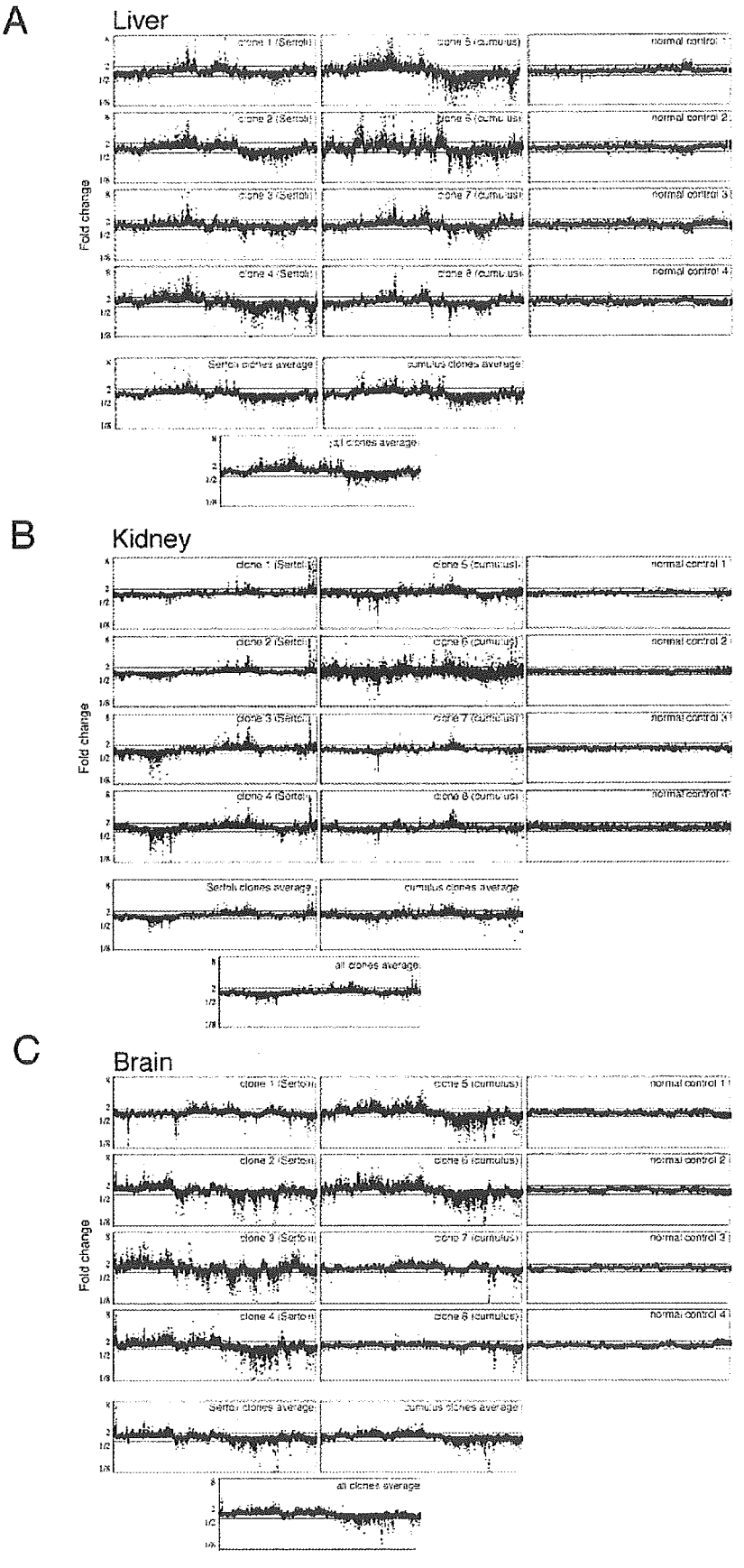

FIG. 1. Gene expression profiles of somatic cell clones and control mice. The gene expression profiles of somatic cell clones and control mice in the liver (**A**), kidney (**B**), and brain (**C**). The intensity of each signal from the DNA microarray was normalized by dividing it by the mean signal intensity of the normal controls. If the value exceeded 1, this value was used as the fold increase; if the value was less than 1, the inverse was used as the fold decrease. To calculate the fold change for each normal control, the mean values were calculated from the data for the other three controls to avoid underestimation. Genes with similar expression patterns among the cloned individuals were clustered using Cluster 3.0, and the fold increase or decrease was plotted in the gene order resulting from the cluster analysis. Each graph represents the data from one cloned or normal individual (upper 12 panels; four Sertoli cell-derived clones, c1(s) to c4(s); four cumulus cell-derived clones, c5(c) to c8(c); and four normal controls, n1–n4). The three lower panels show the mean fold changes for the Sertoli cell clones, the cumulus cell clones, and for all cloned individuals. The red dots represent genes of which expression levels exceeded a two-fold change in all of the individual clones. Note that the gene orders among liver (**A**), kidney (**B**) and brain (**C**) differ because the gene clustering was carried out independently.

TABLE 1. The numbers of genes exhibiting increased or decreased expression levels in each clone and control individual.

Tissue	c1(s)	c2(s)	c3(s)	c4(s)	c5(c)	c6(c)	c7(c)	c8(c)	n1	n2	n3	n4
Liver												
Up[a]	275	441	195	697	913	791	316	287	45	19	21	10
Down[b]	191	565	224	911	1159	771	316	236	29	145	51	23
Changed[c]	466	1006	419	1608	2072	1562	632	523	74	164	72	33
Kidney												
Up[a]	188	246	298	414	235	839	95	207	4	21	3	51
Down[b]	52	154	560	568	357	929	124	202	77	138	93	81
Changed[c]	240	400	858	982	592	1768	219	409	81	159	96	132
Brain												
Up[a]	231	699	1101	817	883	918	240	22	5	7	110	94
Down[b]	263	882	1186	1099	1191	1184	250	188	147	95	119	95
Changed[c]	494	1581	2287	1916	2074	2102	490	210	152	102	229	189
Total[d]												
Up[a]	666	1232	1410	1621	1590	2063	589	471				
Down[b]	468	1356	1583	1884	1826	2105	642	470				
Changed[c]	1134	2588	2993	3505	3416	4168	1231	941				

[a] Upregulated by at least two-fold.
[b] Downregulated to less than half.
[c] The sum of the numbers of up- and downregulated genes.
[d] The sum of the number of genes with altered expression in the three tissues, without duplicates.

software. The signals were normalized using the qspline algorithm implemented in the Bioconductor package of the statistics program R [15]. Genes with similar expression profiles were clustered and displayed using Cluster 3.0 and Java TreeView, originally developed by Eisen et al. [16]. The data from the individual microarrays are accessible for download through the National Center for Biotechnology Information's Gene Expression Omnibus (http://www.ncbi.nlm.nih.gov/geo/) via series accession number GSE3128.

Quantitative Reverse Transcription-Polymerase Chain Reaction

Genomic DNA and total RNA were prepared from neonatal tissues of the Sertoli cell- and cumulus cell-derived clones and from normal controls using ISOGEN (Nippon Gene), as described previously [17]. All RNA samples were treated with RNase-free DNase I. The cDNA was synthesized from 1 μg total RNA using Superscript II reverse transcriptase (Life Technologies) with an oligo(dT) primer. For reverse transcription-polymerase chain reaction (RT-PCR), 1 ng cDNA in a 100-μl reaction mixture containing 1× ExTaq buffer (TaKaRa), 2.5 mM dNTP mixture, primers, and 2.5 U ExTaq enzyme (TaKaRa) was subjected to 30 PCR cycles at 96°C for 15 sec, 65°C for 30 sec, and 72°C for 30 sec on a Perkin Elmer GeneAmp PCR system 9600. Target

TABLE 2. The numbers of genes in each of the donor cell types exhibiting a two-fold or greater difference in mean expression level that was significantly different from the controls.[a]

Tissue	Sertoli clone-specific	Cumulus clone-specific	Sertoli and cumulus clones
Liver			
Up	119	154	54
Down	121	128	99
Changed	240	282	153
Kidney			
Up	169	58	20
Down	80	69	26
Changed	249	127	46
Brain			
Up	16	24	1
Down	23	27	4
Changed	39	51	5
Liver and kidney			
Up	5	4	0
Down	4	10	2
Changed	9	14	2
Kidney and liver			
Up	1	1	0
Down	0	0	0
Changed	1	1	0
Brain and liver			
Up	3	3	1
Down	0	0	0
Changed	3	3	1
Liver, kidney, and brain			
Up	0	0	0
Down	1	1	1
Changed	1	1	1

[a] Differences were tested using Student *t*-test ($P < 0.05$). The numbers of genes with altered expression levels in all tissues are also shown.

TABLE 3. Genes exhibiting increased expression levels in the kidneys of Sertoli cell-derived clones.

Gene name	Average fold change in Sertoli clone	Average fold change in cumulus clone
Fgg	12.65	1.07
Alb1	11.37	0.36
Apoa2	10.69	1.56
Trf	9.33	0.91
Vtn	8.91	1.09
Ahsg	8.72	0.53
Fga	7.57	2.33
Apoa1	7.31	0.59
Serpina1d	6.41	1.36
Rbp4	6.41	2.02
Fetub	6.38	1.37
Fgb	6.31	0.58
Bhmt	6.08	1.65
Sedrpina1a	5.97	0.85
Serpinc1	5.50	0.47
Hp	4.97	1.40
Itih3	4.93	0.79
Ambp	4.67	1.28
Serpina1e	4.06	0.73
Fabp1	3.89	0.36
Pon1	3.54	1.12
Vnn3	3.52	1.31
Serpina3n	3.29	2.19
NM_015779	3.16	0.96
Apoc4	3.13	0.68
Itih1	3.07	0.89
Tmod1	2.87	0.93
Ttr	2.85	1.73
Serpina1b	2.72	1.24
Uox	2.69	0.83
Mug1	2.53	0.95
Asgr1	2.49	0.98
Rhced	2.46	0.94
Lrg	2.29	2.64
Hpxn	2.24	0.90

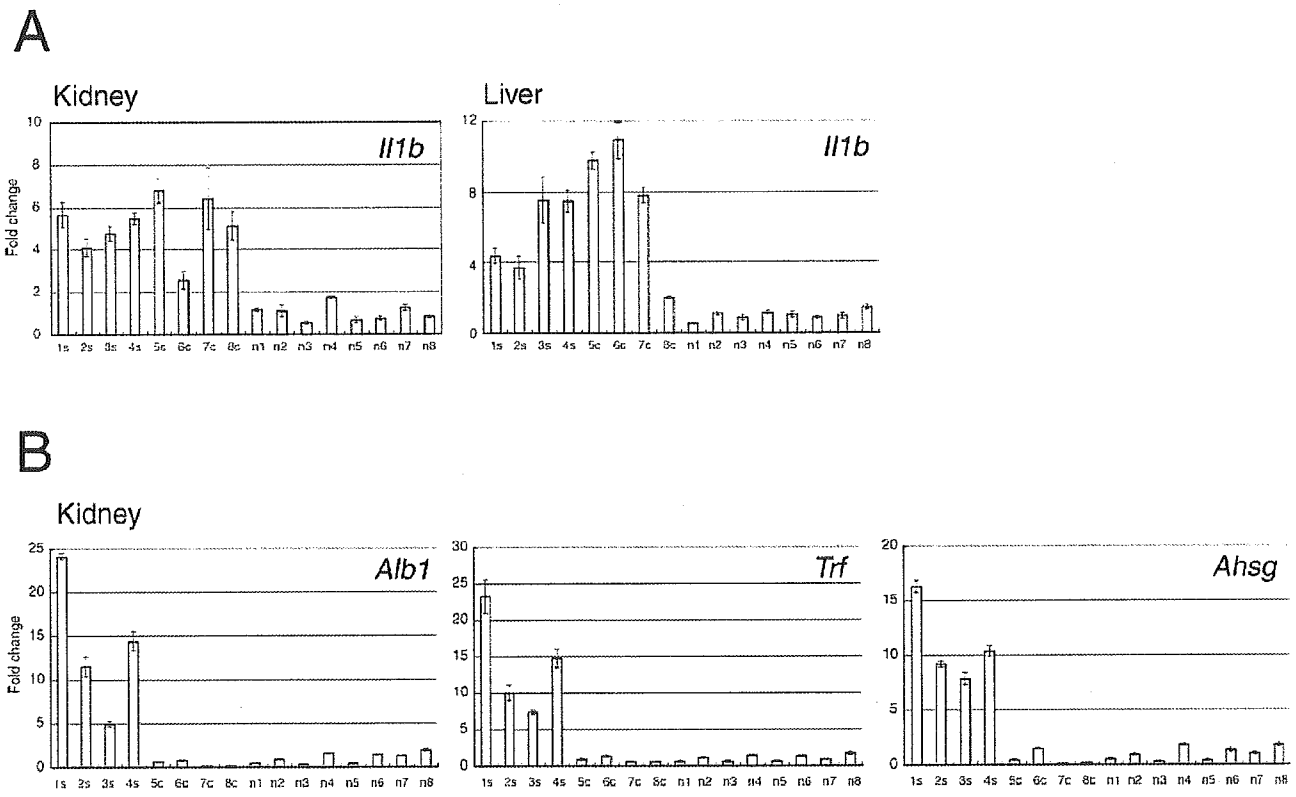

FIG. 2. Genes exhibiting donor cell-independent and -dependent dysregulation effects. The gene expression levels were determined using quantitative RT-PCR in triplicate and normalized using the detected expression level of *Actb*. The mean level of gene expression in the normal controls was set to 1. The standard errors are shown using error bars. A) The expression levels of interleukin 1 beta (*Il1b*) in the liver and kidney. *Il1b* was 1 of 200 genes exhibiting increased expression in all eight clones. B) The expression levels of three genes exhibiting abnormal expression in the kidney that were Sertoli cell clone-specific. *Alb1*, albumin; *Trf*, transferrin; *Ahsg*, alpha-2-HS-glycoprotein.

cDNA fragments were cloned into plasmids to use as standards in the quantitative analysis of gene expression. The primers used for quantification were *Alb1*-F, 5′-TCA GAG ACT GCC TTG TGT GG-3′; *Alb1*-R, 5′-CAG CCT TGC AAC ATG TAT CC-3′; *Trf*-F, 5′-GTC CTG GAT AAC ACC GAA GG-3′; *Trf*-R, 5′-ACA GAT TGC ATG TAC TCC GC-3′; *Ahsg*-F, 5′-ATA GCC ACC ACT GAA GCT GG-3′; *Ahsg*-R, 5′-TGA AGA TTG GCA AGA GCA CC-3′; *Actb*-F, 5′-AAG TGT GAC GTT GAC ATC CG-3′; and *Actb*-R, 5′-GAT CCA CAT CTG CTG GAA GG-3′. The gene expression levels were measured using an ABI PRISM 7700 detection system and SYBR Green PCR Core Reagents (Applied Biosystems). No amplification of RT-PCR products was detected in the reverse transcriptase-minus controls.

RESULTS

Using DNA microarrays, we analyzed the gene expression profiles of the liver, kidney, and brain tissues of four neonatal clones derived from immature Sertoli cells, four neonatal clones derived from cumulus cells, and four neonatal normal control mice produced by in vitro fertilization. Figure 1A illustrates the gene expression profiles of the liver for each individual. The fold change in the expression level of each gene in each animal was calculated relative to the mean expression level of the corresponding gene in the four normal control individuals. The results were plotted in the gene order derived from the cluster analysis of the expressed genes in the microarray. It was apparent that, in the normal controls, the expression of all genes was tightly regulated within a factor of two (as indicated by the horizontal lines in each panel of Fig. 1A) for each individual. Therefore, the overall pattern of gene expression was uniform, with little divergence among the normal control individuals (Fig. 1A, right panels). In contrast, in the clones derived from Sertoli (Fig. 1A, left panels) and cumulus (Fig. 1A, middle panels) cells, many genes were expressed abnormally in each clone, and the gene expression profiles were divergent among the cloned individuals. In all clones, between 4% and 20% (419-2072 of the 10 012 genes in the microarray) of the genes exhibited a more than two-fold increase or decrease in signal intensity compared with the mean expression level in the controls (Table 1). The extent of abnormal gene expression in the kidney and brain was similar to that in the liver (2–20%; Table 1 and Fig. 1, B and C).

These analyses demonstrated the existence of genes exhibiting both donor cell-dependent and -independent effects on expression in somatic clones, as has been reported previously [8]. Approximately 200 genes were up- or down-regulated in the same manner in both types of clone in at least one of the three tissues (Table 2). For example, the expression of *Il1b* was upregulated in the liver and kidney of both the cumulus cell- and Sertoli cell-derived clones (Fig. 2A).

Interestingly, in the class II major histocompatibility complex (MHC) region on chromosome 17, seven genes within a 500-kilobase (kb) region exhibited increased expression levels in the liver, including class II MHC and MHC-related genes (Fig. 3A).

In the analysis of gene expression in the kidney, approximately 35 genes exhibited increased expression levels that were specific to the Sertoli cell-derived clones (Table 3), apart from male-specific genes that showed common expression in Sertoli cell-derived clones and male control individuals, and were mapped on the Y chromosome. This group included